THESIS

APPLICATION OF TIME-LAPSE TTEM FOR GROUNDWATER MONITORING AND RECHARGE IN THE SAN LUIS VALLEY, COLORADO, USA

Submitted by

Julianne Robinson

Department of Civil and Environmental Engineering

In partial fulfillment of requirements

For the Degree of Master of Science

Colorado State University

Fort Collins, Colorado

Summer 2025

Master's Committee:

Advisor: Ryan G. Smith

Michael Ronayne
Antonio Alves Meira Neto

Copyright by Julianne E. Robinson 2025

All Rights Reserved

ABSTRACT

APPLICATION OF TIME-LAPSE TTEM FOR GROUNDWATER MONITORING AND RECHARGE IN THE SAN LUIS VALLEY, COLORADO, USA

The ability to measure groundwater availability, extraction, and recharge is becoming increasingly important as the climate changes and reliance on groundwater in water-stressed regions increases. Geophysical measurement methods like time-domain electromagnetic (TEM) surveys can address the need for cost-effective, high-resolution hydrostratigraphic data collection with greater spatial and temporal coverage than direct-sampling methods. Among other applications, these data can be used to map hydrostratigraphy and improve targeting of managed aquifer recharge. The application of TEM surveys for time-lapse studies could enable an expansion of the spatial and temporal scales of geophysical measurements, enhancing the capabilities in hydrologic applications such as delineating the infiltration front from groundwater recharge. Few studies have used mobile TEM surveys for time-lapse measurements. This study used geophysical datasets collected with towed time-domain electromagnetic (tTEM) surveys to track changes in subsurface resistivity at managed groundwater recharge sites in the San Luis Valley in south-central Colorado. Study sites were surveyed with tTEM approximately every six weeks over the course of the irrigation season to provide time-lapse datasets. Geostatistical tools were utilized to account for differences in measurement locations from survey to survey. Results show changes in subsurface resistivity consistent with recharge flows and observed soil water content throughout the irrigation season. Infiltration of recharge water at the study site followed lateral downward paths and was controlled primarily by the volume of recharge water applied.

Minor variations were observed in lithology at depth, but the site had few geologic barriers to infiltration, making it a suitable location for managed recharge. This study demonstrates the capability of tTEM surveys to efficiently assess groundwater recharge over time through analysis of time-lapse measurements. This information can serve as an important addition to other forms of data to inform water management strategies, including managed aquifer recharge, in the San Luis Valley and other arid and semi-arid regions dependent on groundwater.

ACKNOWLEDGEMENTS

I would like to acknowledge and thank the many people and organizations who made this research possible. First, I would like to thank my advisor, Dr. Ryan Smith, for his support, guidance, and feedback throughout my work on this project. Thanks to Dr. Michael Ronayne and Dr. Antonio Alves Meira Neto for serving on my committee and providing valuable insights.

This project involved collaboration among researchers, consultants, and stakeholders in the San Luis Valley. Special thanks to Trevor Harmon and Taylor Chick for their support in the field, and to Patrick O'Neill for sharing his knowledge on water resources and farming in the San Luis Valley. I would also like to thank Rahel Pommerenke, Matt Cipra, Kajsa Holland-Goon, Fahim Hasan, Susmita Pant, Victoria de Souza Wojahn, James Molloy, Dawit Asfaw, and Abdullah Al Fatta for their help with field work. This project would not have been possible without their generous contributions of time and effort.

Thanks to Dr. Gregory Butters, Dr. Christopher Bareither, Dr. Jeremy Rugenstein, Dr. Jeffrey Niemann, Dr. Jiawei Li, Holly Proulx, and John Toy for their support with training, lending field equipment and laboratory space, and assisting with equipment calibration and maintenance.

I would like to express my appreciation to the donors of the scholarships I received during my time at CSU: the Colorado Groundwater Association's Harlan Erker Memorial Scholarship, the Tipton and Kalmbach/Stantec Graduate Fellowship, and the Whitney Borland Scholarship. The generous financial support from these organizations helped make this project and my graduate studies possible.

Finally, I would like to thank my family and friends for their encouragement and support throughout my time in graduate school, especially my mother, Carmen, and father, Don.

TABLE OF CONTENTS

LIST OF TABLES

LIST OF FIGURES

1. INTRODUCTION

1.1 Background

There is a growing need to characterize and monitor groundwater resources as the climate changes and demand for water increases, particularly in arid and semi-arid regions of the world that depend on groundwater for irrigated agriculture and domestic water supply. Adapting water use and management to changing conditions in the future is essential for ensuring the sustainability of these regions. Irrigation supplied by groundwater comprises a large portion of agricultural production in the United States and other parts of the world. Irrigated agriculture is the primary use of land and a cornerstone of the local economy in the San Luis Valley (SLV) in south-central Colorado. Irrigation in the SLV relies heavily on groundwater supplies due to the hydrology of the region. Sustainable groundwater management is necessary for agricultural, economic, and ecological health, and it impacts downstream water users, including stakeholders in interstate water compacts, in the case of the Rio Grande Basin (CWCB 2025).

Managed aquifer recharge (MAR) is an increasingly important tool for addressing groundwater depletion, and interest in its application has grown with the need for improved groundwater sustainability. Success of MAR depends on site-specific hydrogeologic characteristics, and assessing site feasibility to the extent needed for targeted design of recharge facilities is often costly and time-consuming. Geophysical surveys can enable rapid, non-invasive site characterization and assessment for the study, design, and implementation of aquifer recharge facilities, facilitating MAR in places where it might otherwise be unattainable.

Geophysical methods commonly used in hydrological applications include induced polarization, self-potential, ground penetrating radar, electrical resistivity, electromagnetic

induction (of which tTEM is one method), seismic refraction, nuclear magnetic resonance, and microgravity methods (Binley et al., 2015). Previous geophysical studies at other locations in the SLV have successfully used electrical resistivity tomography (ERT) (Zeigler Geologic Consulting LLC et al., 2020), gravity methods (Keller et al. 1984), ground-based TEM (Fitterman et al., 2010), and airborne electromagnetic (AEM) (Ball et al., 2015) surveys to map hydrostratigraphy. However, these methods are limited in either spatial or temporal scales; AEM surveys do not provide information at the resolution needed for developing field-scale recharge site design, and commonly used ground-based geophysical tools can be cost-prohibitive and time-consuming even for small-scale applications.

This study implemented a novel approach for applying towed time-domain electromagnetic (tTEM) surveys to characterize hydrostratigraphy and track groundwater infiltration over the course of an irrigation season. Towed time-domain electromagnetic (tTEM) surveys employ similar technology as other EM techniques with the advantage of greater spatial coverage than ERT and higher resolution of shallow (<10m) layers than AEM (Auken et al., 2019).

The tTEM survey system has a lateral resolution of 10 m and is capable of imaging up to a depth of 70 m in clay-rich environments (Christiansen and Auken, 2012), which makes it suitable for surveying areas from a few hectares up to 10 km^2 (field scale) within a reasonable time and cost (Auken et al., 2019). Behroozmand et al. (2019) describe some of the advantages of using tTEM over other geophysical methods for MAR site assessment, among them the measurement of electrical resistivity (as opposed to other characteristics) to delineate water flow paths, its cost-effectiveness, and a data resolution that is well-suited to a field scale typical of

MAR projects. To the author's knowledge, the tTEM system has not previously been used for a time-lapse study.

1.2 Time-Lapse Geophysics

Time-lapse geophysical studies commonly rely on direct current resistivity methods, which are well-suited to time-lapse measurements (Loke et al., 2013; Singha et al., 2015; Slater and Binley 2021). For example, ERT has been implemented to measure groundwater recharge processes over time including infiltration of irrigation water (Scaini et al., 2017), water for soil aquifer treatment (Haaken et al., 2016), snowmelt (Thayer et al., 2018), karst vadose zone recharge (Watlet et al., 2018), and unsaturated flow at the hillslope scale (Kotikian et al., 2019), among other applications.

The use of transient electromagnetics for time-lapse measurements has developed more recently. Geophysical methods based on electromagnetic induction have the advantage of a greater spatial scale compared to direct current methods, and differences in resolution make this approach better suited to certain applications, including field-scale MAR studies. El-Kaliouby et al. (2007) presented an early use of TEM for time-lapse infiltration monitoring; their field-scale study found that the method could detect changes in infiltration over time, although uncertainties remained about the ability of the method to constrain quantitative analyses. Swidinsky & El-Kaliouby (2013) used time-lapse TEM to monitor infiltration on a field scale and hypothesized that using a constrained inversion based on a priori data would improve the accuracy of the results. Chen et al. (2019) used time-lapse TEM to monitor groundwater movement between aquifer units, providing data beyond what could be acquired through pump tests or hydrogeological methods. King et al. (2022) simulated repeat AEM surveys to estimate hydrogeological parameters and map groundwater salinity distributions. They demonstrated that

repeat AEM surveys could be used to estimate these parameters through a coupled time-lapse hydrogeophysical inversion, with the assumption that surveys were repeated in the same location each time.

The above-mentioned studies all made use of spatially static or collocated surveys. The implementation of mobile TEM tools such as the tTEM for time-lapse studies faces barriers due to differences in data acquisition locations. Huang and Cogbill (2006) demonstrated that AEM surveys can be repeated for time-lapse measurements, and the AEM method offers good repeatability if repeated flightline paths are spatially consistent and the inverted data (apparent resistivity) are compared, rather than the electromagnetic response itself. However, if flight paths are spatially inconsistent, repeatability of surveys is expected to be poor because small variations in sensor altitude or plan-view flight path can cause large changes in the EM response (Huang and Cogbill, 2006). Xiao et al. (2022) developed an inversion scheme for 3-dimensional time-lapse TEM data that addressed challenges associated with non-collocated data and non-optimal data coverage. They used two TEM datasets collected with a one-year interval and emphasized the importance of careful selection of regularization settings in inversions due to their notable impacts on results.

McLachlan et al. (2023) point out the importance of TEM data quality for detection of subtle hydrological processes; the presence and influence of noise must be well understood to accurately monitor dynamic processes. Zamora-Luria et al. (2023) introduced a monitoring TEM (mTEM) system capable of long-term measurements for studying seasonal patterns in groundwater dynamics. This system employed a time-constrained inversion based on a laterally constrained inversion scheme and relied on a semi-permanent installation to ensure that observed changes were the result of dynamic processes rather than differences in measurement locations.

These studies lay the groundwork for the implementation of TEM methods for time-lapse measurements, but challenges and limitations related to the inversion process and measurement consistency remain to be addressed. The use of towed TEM for time-lapse measurements stands to serve as a valuable tool to inform groundwater management by providing rapid quantification of changes in vadose zone saturation over larger areas than other geophysical methods. Previous studies utilizing towed TEM surveys have focused on one-time, standalone measurements; the system has not been sufficiently tested in a time-lapse capacity, warranting further investigation of its capability to provide insight into time-varying hydrologic processes.

1.3 Research Objectives

The objective of this study was to track changes in subsurface resistivity due to canal and flood recharge efforts at the study site through repeat tTEM surveys over the course of the irrigation season. Subsurface resistivity was used as a proxy for saturation to understand recharge timing and its impact on water levels. This information can contribute to the assessment of site suitability for MAR. Groundwater flow pathways in the study region were expected to be controlled primarily by transitionally deposited clay layers, where present, and regional fluctuations in the water table in the absence of confining clays. Previous hydrogeological studies of the region have shown that stratigraphic permeability along the west side of the SLV is highly variable, depending largely on the degree of sediment sorting and grain size near the mountain front (Huntley 1979). This variability makes it difficult to predict recharge dynamics on a field scale without site-specific investigation. The study site's proximity to an unlined canal and recharge pond made it an ideal location to test the use of tTEM for time-lapse measurements – seepage from the canal and recharge pond improved the likelihood of detecting changes in saturation compared to what would be expected in a natural setting.

A key challenge in using tTEM for time-lapse analysis lies in the inversion process used to convert raw data into hydrogeologically useful information when survey locations vary across acquisitions. This study applied laterally constrained inversions and used 3-dimensional empirical Bayesian kriging to account for non-coincident acquisition locations, providing a record of changes in subsurface resistivity throughout the irrigation season.

1.4 Study Area

This study focused on a site located at the base of the San Juan mountains on the western side of the San Luis Valley, Colorado. Figure 1 shows the study site location. The Rio Grande Canal runs adjacent to the area surveyed with the tTEM and is filled via a diversion from the Rio Grande River near Del Norte, Colorado. Gage measurements in the canal indicate that the canal contained water from April 1-November 1, 2024, with a brief shutoff from August 1-6, 2024, due to low flows in the Rio Grande River. The Rio Grande Canal is unlined and serves as a source of recharge water for the unconfined aquifer. A constructed recharge pond exists on the southwestern edge of the field site and was utilized periodically in the 2024 irrigation season. Exact records of the timing of water deliveries to the recharge pond were not available but corresponded to times of higher flows in the Rio Grande Canal; between April and September 2024, a total of approximately 246 ac-ft. (3×10^5 m^3) of water was delivered to the recharge pond. Of this, the largest amount of water was delivered in July (Q. Norris, personal communication, 2025).

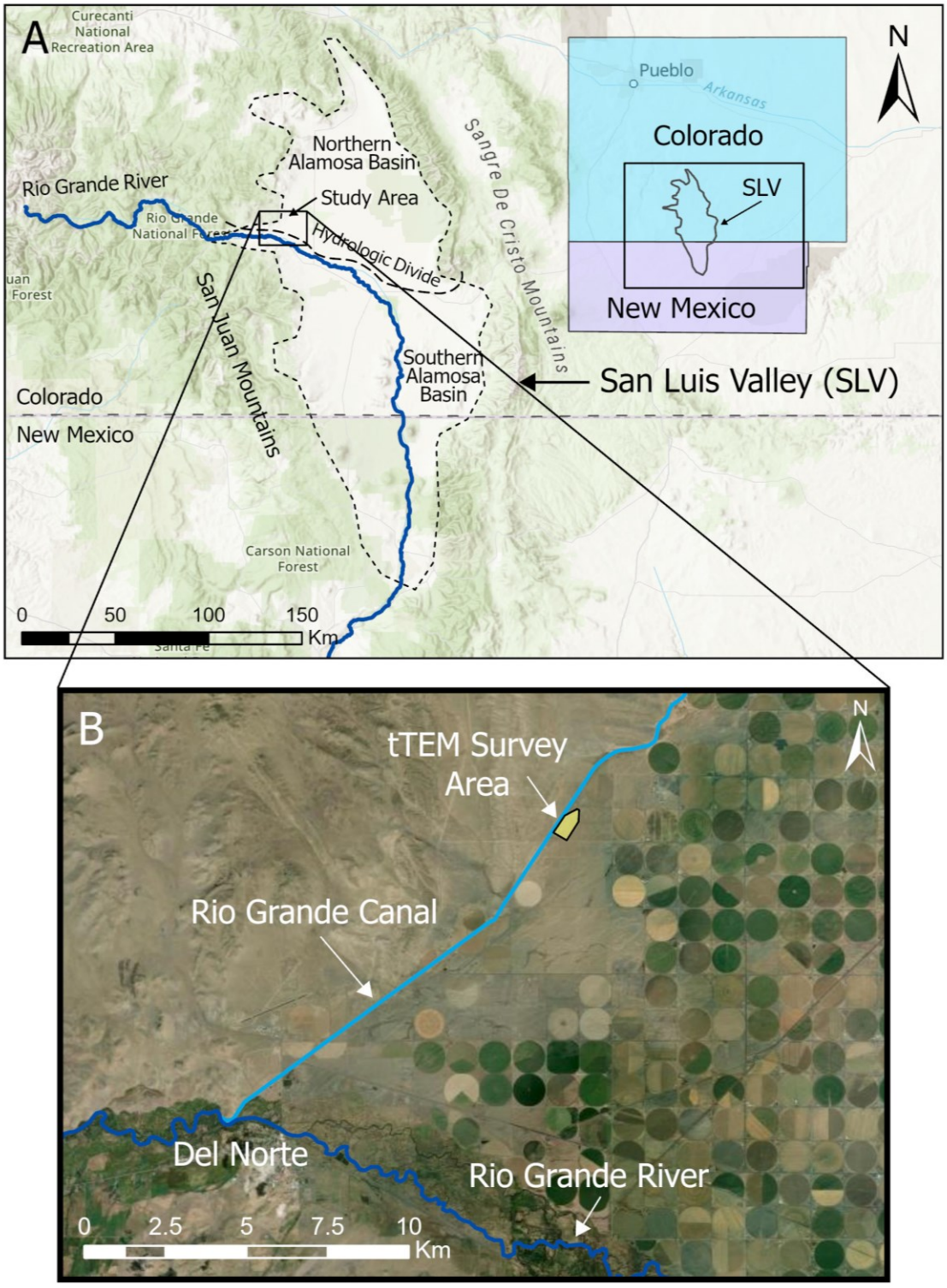

Figure 1: A) Site map showing the study area in south-central Colorado to the east of the San Juan Mountains; B) Study site northeast of Del Norte shaded in yellow, with Rio Grande Canal and Rio Grande River. Imagery sources: ESRI World Topographic Map and ESRI World Imagery.

1.4.1 Hydrology of the San Luis Valley

The San Luis Valley is an arid intermontane basin, covering approximately 8,100 km^2 with an average elevation of 2336 m above mean sea level (amsl). The region receives an average of 18-25 cm of precipitation annually (Harmon 2020). Approximately 86 percent of incoming surface water (derived from surface inflows and precipitation) is lost through evapotranspiration. Remaining water leaves the system through groundwater flow, or (with the exception of the endorheic Northern Alamosa Basin), surface water flow (Sunada et al., 1983). Natural recharge occurs at the edge of the valley through mountain front recharge on the surface and through bedrock formations as mountain block recharge. Figure 2 shows a cross section detailing subsurface geology and generalized groundwater flow paths on the western side of the valley.

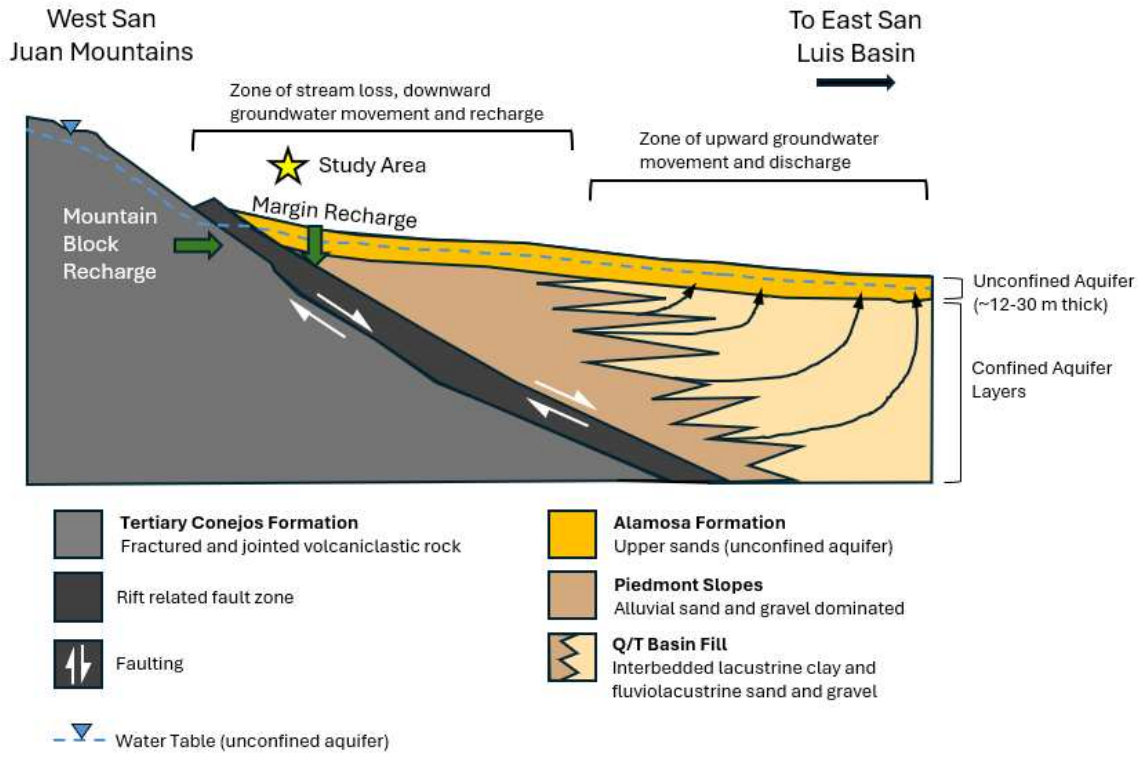

Figure 2: Conceptual model of the west-central SLV (modified from Wasiolek 1995, Hawley and Kernodle 2000, and Beetle-Moorcroft et al., 2021, as shown in Harmon 2020). Not to scale.

The two main aquifer units in the San Luis Valley are a shallow unconfined aquifer and a highly prolific confined aquifer. Both are primarily in the Alamosa Formation (Barkmann et al., 2020), which is composed of Pleistocene and Holocene-era clay-rich lacustrine deposits interstratified with fluvial sands (Siebenthal 1910; Huntley 1979; Sunada et al., 1983). A series of clay deposits (locally referred to as the "blue clay") form a boundary between the unconfined and upper confined aquifers. Depth to the confining layers ranges from approximately 12-30 m below ground surface (bgs), from the southern to the northern part of the valley, respectively (Barkmann et al., 2020). Depth to the first confining layer has been observed as shallow as 6 m and as deep as 60 m in some places (Harmon 2020). The confining clay series does not extend fully to the edges of the valley (HRS Water Consultants Inc. 2002); on the western edge of the SLV, the confining clay pinches out against coarse-grained alluvial and volcanic sediments (Huntley 1979). A deeper, less productive confined aquifer has been identified in some parts of the basin (Fitterman et al., 2006). Hydraulic conductivity is relatively high in the alluvium and fan deposits at the edges of the valley and decreases towards the center of the Alamosa Basin (Harmon 2020). Notably, horizontal hydraulic conductivity has been found to exceed vertical hydraulic conductivity by one to four orders of magnitude in alluvial sediments on the western edge of the SLV (Huntley 1979; Bexfield and Anderholm, 2010). Natural recharge in the unconfined aquifer comes primarily from mountain block recharge (Figure 2), precipitation, and streambed infiltration. Other sources of recharge include unlined irrigation canals extending throughout the valley and irrigation return flows (Barkmann et al., 2020).

1.4.2 Water Use and Management in the San Luis Valley

The SLV is one of Colorado's most productive agricultural regions. Irrigation makes up the largest use of water in the SLV and is necessary for agriculture to be viable (Harmon 2020). Irrigation water is drawn from a combination of surface water and groundwater fed from runoff of snowmelt and precipitation in the San Juan, Tusas, and Sangre de Cristo Mountain Ranges surrounding the valley (Harmon 2020). Understanding the factors that influence mountain front recharge is increasingly important for informing water management as precipitation and snowmelt patterns change. Various numerical models have been developed to estimate the impacts of groundwater use since intensive groundwater use began in the early 1900s. Updated groundwater models and response functions are developed by the Colorado Division of Water Resources' Rio Grande Decision Support System, RGDSS (Harmon 2020). The volumes of water contributed by recharge processes are often difficult to quantify due to limited data availability (Markovich et al., 2019).

Administration of water in the Rio Grande Basin is governed by both Colorado state law and the Rio Grande Compact, a 1938 agreement between Colorado, New Mexico, and Texas that stipulates shared governance of the Rio Grande's waters (Barkmann et al., 2020). The State of Colorado administers water rights through the doctrine of prior appropriation. The passage of the Colorado Ground Water Law in 1957 required water users to obtain a permit prior to constructing large capacity (>50 gallons per minute [gpm]) wells; prior to this, groundwater use in Colorado was not regulated. The Water Rights Determination and Administration Act of 1969 further specified actions to manage water rights related to the use of groundwater. Although these compacts and laws were passed in the 20th century, development of water in Colorado and the San Luis Valley began decades earlier (Barkmann et al., 2020).

Permanent irrigation structures were installed in the San Luis Valley beginning in the mid-1800s. In the century that followed, irrigation activities relied primarily on surface water flows that fluctuated from year to year and were insufficient in times of drought. The invention of center pivot irrigation systems and improved pump technology in the mid-1900s shifted this reliance to groundwater (SWAG 2023) and enabled an expansion of irrigated agriculture in the region.

It was known that wells in the region were impacting surface water supplies, based on anecdotal evidence (Simpson 2018), but the extent was not well understood. In 1972 the State of Colorado issued a moratorium on wells in the confined aquifer. In the same year, the Federal Government worked with local partners to develop the Closed Basin Project, which had the goal of capturing water in areas of surplus in the Northern Alamosa Basin and delivering it to the Southern Alamosa Basin, where it could be used to supplement water supplies to meet Colorado's obligation to New Mexico and Texas as part of the Rio Grande Compact of 1938. This was intended as a form of mitigation to compensate for impacts to the Rio Grande Compact from pumping in the closed basin. The Rio Grande Water Conservation District (RGWCD) began monitoring water levels in wells throughout the SLV in 1976. In the early 1980s, the State issued a moratorium on wells in the principal unconfined aquifer (Simpson 2018). In response to drought in 2002, many irrigators made the switch from flood to sprinkler irrigation to increase the efficiency of water use (Phillips 2021).

The Rio Grande Water Conservation District formed water user-managed subdistricts in 2010, each responsible for developing their own groundwater management plan. The groundwater management plans are collective agreements for how subdistricts plan to facilitate replacements for injuries to senior surface water rights holders caused by well pumping. New

appropriations from the confined aquifer require an augmentation plan (Barkmann et al., 2020). Subdistricts fund water acquisition to mitigate depletions from pumping and buy or lease land to remove it from agricultural production (Harmon 2020).

The San Luis Basin is also required by the State of Colorado to maintain sustainable aquifers, defined by location-specific groundwater levels. Subdistrict No. 1 operates under a court decree that requires the unconfined aquifer to be recovered to a benchmark, through voluntary programs, by 2030. Figure D1 in Appendix D shows the required recovery in the unconfined aquifer, and the changes in unconfined aquifer storage in the west central part of the SLV from 1976-2024. If this requirement is not met, regulatory action will be taken by the State Engineer to shut down wells in the region to curtail pumping. Although this could lead to aquifer recovery given adequate time, it would have negative socioeconomic impacts on the region (Simpson 2018).

As of 2001, a total of approximately 10,000 wells have been completed in the valley, 90 percent of which are used for crop irrigation. Between 1969-1980, water level declines of up to 12 m were observed in the unconfined aquifer. It is estimated that the unconfined aquifer has lost 1 million ac-ft (1.2×10^9 m^3) of storage since 1976 (Barkmann et al., 2020). In 2010, approximately 43 percent of groundwater pumping in the San Luis Basin drew from the unconfined aquifer, while 57 percent came from the confined aquifer. Groundwater pumping in the Northern Alamosa Basin that year accounted for approximately 65 percent of all groundwater diversions in the San Luis Valley. About 37 percent of this volume was derived from the unconfined aquifer, while 28 percent came from the confined aquifer (Harmon 2020).

Numerous studies have characterized the geology and hydrology of the San Luis Valley and provide a good overview of overarching structures and processes. However, distilling this

information down to the field scale, a necessary step in assessing the feasibility of MAR or other groundwater management strategies or developing groundwater models to inform management (among other applications) is difficult due to spatial heterogeneity. Local hydrogeology is varied, complex, and remains poorly understood in certain areas; correspondingly, site-specific information cannot be extrapolated because many of the hydrologically important geologic layers are not regionally extensive (Kuenhold 2004). This justifies the need for field-scale investigations when site-specific information is needed.

1.4.3 Study Site Characteristics

The study site is in the Northern Alamosa Basin or "Closed Basin", an internal drainage that does not contribute any natural surface water flow and little to no unconfined aquifer groundwater flow to the Rio Grande River to the south. This area is designated by the Rio Grande Water Conservation District as Subdistrict No. 1. Subdistrict 1 covers the area of highest groundwater use for irrigation in the San Luis Valley (SWAG 2023). Figure 1 in Section 1.4 shows the location of the Northern Alamosa Basin in the valley.

The study site was used in 2024 by the Rio Grande Water Conservation District (RGWCD) as a location for managed recharge of the unconfined aquifer. Three wells within a 1-km radius of the survey area were used to acquire information on lithology and water levels. Figure 3 shows a map of the study site, including nearby wells, the pond used for managed recharge at the site, the Rio Grande Canal, and the area surveyed with the tTEM system.

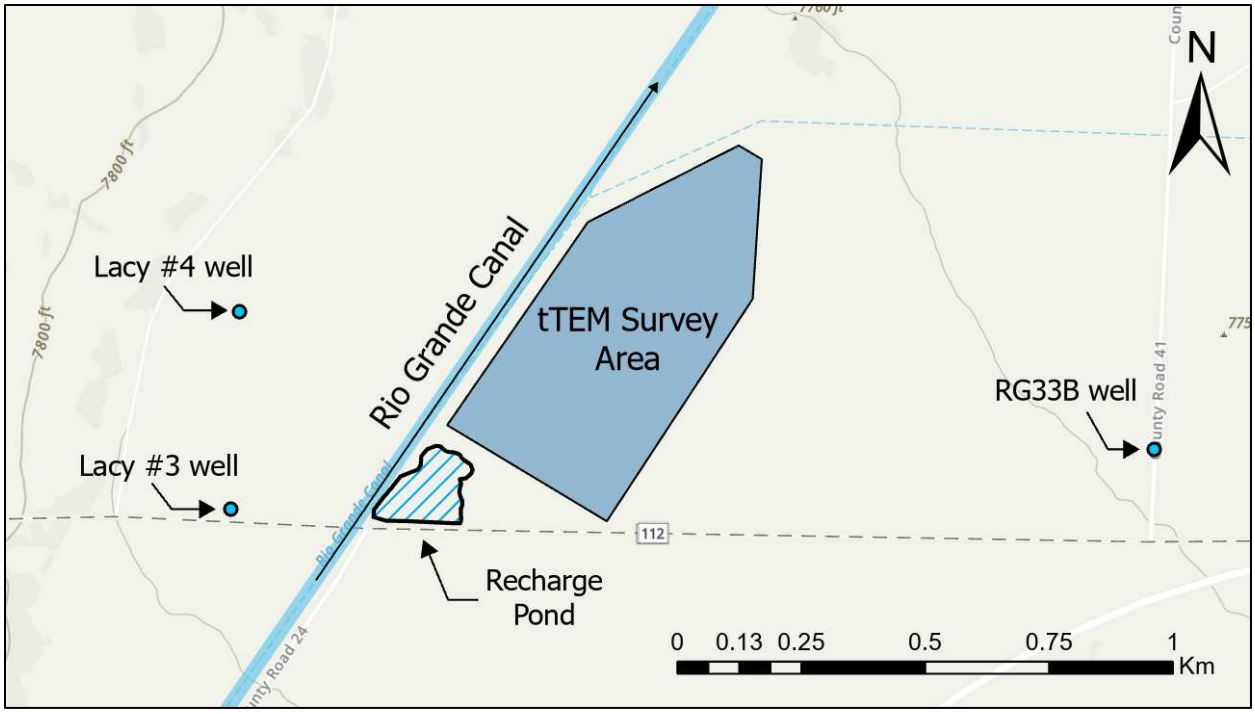

Figure 3: Site map showing the study area and nearby wells used to acquire lithology and water level data. Imagery source: ESRI World Topographic Map.

The Lacy #3 and Lacy #4 wells were developed as irrigation wells, while the RG33B well was developed as a monitoring well. Table 1 shows the completion dates, total depths, and perforated depth ranges for the Lacy #3, Lacy #4, and RG33B wells.

Table 1: Construction date, completed depth, and perforated depth range for wells in Figure 3. Dates are listed in mm/yyyy format.

Well Name	Date Completed	Total Depth	Perforated Depth Range
Lacy #3	08/1943	27 m	25-27 m
Lacy #4	10/1998	46 m	24-46 m
RG33B	12/1998	40 m	27-40 m

Drillers' logs for the Lacy #4 and RG33B wells and the well permit for Lacy #3 are shown in Appendix D (no well log was available for the Lacy #3 well). All three wells are located in the Alamosa Formation and draw from the unconfined aquifer. Both the Lacy #4 and

RG33B well logs describe the lithology as predominantly sand and gravel, with a <1 m thick layer of brown clay at depths of 20 m and 18 m, respectively. In general, hydraulic conductivity (K) is relatively high in the alluvium and fan deposits at the outskirts and decreases towards the center of the valley (Harmon, 2020). Whereas horizontal and vertical hydraulic conductivity can vary considerably in the central part of the basin due to interlayering of gravel-rich and clay-rich deposits, anisotropy at the margins of the basin is relatively low. Lipman (1976) characterized the area directly to the east of the San Juan Mountains as valley alluvium consisting of "silt, sand, gravel, and peaty material", bordered by glacial outwash to the southeast. The glacial outwash is described as "fairly well sorted to well sorted stratified terrace and fan deposits consisting of sand, gravel, and well-rounded boulders" (Lipman 1976). Harmon (2020) describes "coarse, high-energy fan deposits near the San Luis Basin margins", which transition to lower-energy, lower-K fluvial and lacustrine sediments towards the center of the basin. The study site is located at the edge of the basin and falls between the coarse and medium-grained deposits. Given the proximity of the study site to the valley edge, and descriptions of predominantly coarse-grained materials from nearby well logs, it was expected that hydraulic conductivity would be relatively high at the study site.

Groundwater levels in the study area are driven by managed recharge and pumping, both of which occur between April and September. Managed recharge is usually highest from April to June, but varies based on seasonal precipitation and the availability of surface water. Pumping demand follows the growing season and is usually highest from July to August. Monitoring wells in the area provide water level data to observe the aquifer response to recharge, but measurements are spatially constrained, and the movement of water introduced as managed recharge at the study site remained poorly understood prior to this study. Mapping the

hydrostratigraphy of the study area and detecting changes in saturation over time with geophysical surveys can contribute to a better understanding of the effectiveness of managed aquifer recharge processes, which is necessary for sustaining groundwater supply and meeting state-mandated recharge requirements in the San Luis Valley.

2. METHODS

2.1 Survey Instrumentation

This study used the 3x3 tTEM system, which consists of a 3m x 3m transmitter (Tx) coil followed by a receiver (Rx) coil. The layout and dimensions of the 3x3 tTEM are shown in Figure 4 below.

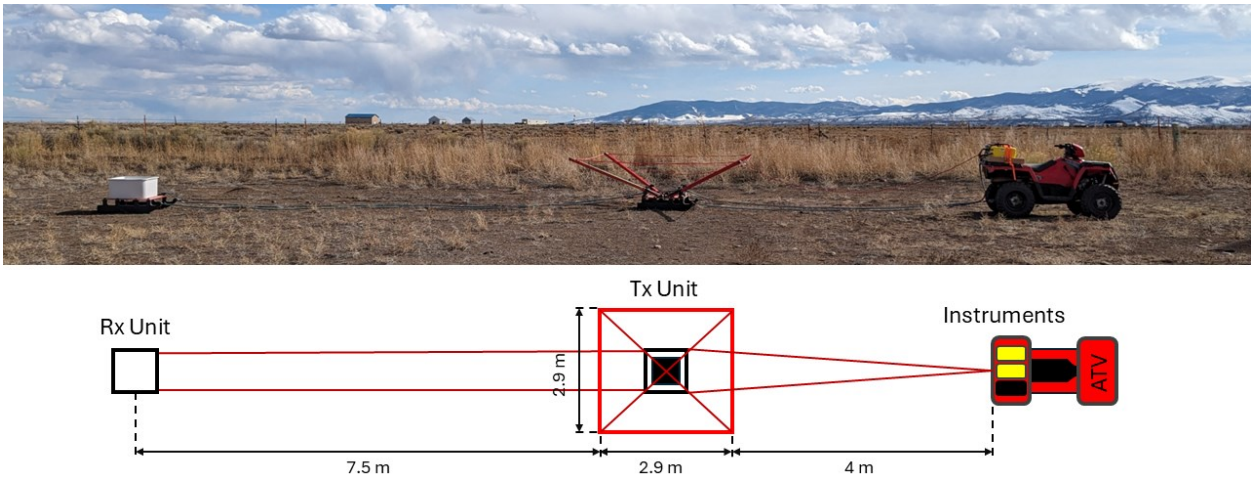

Figure 4: Layout of 3x3 tTEM system.

The tTEM system uses an all-terrain vehicle to tow the Tx frame and Rx coil. Direct current (DC) current is passed through the Tx loop, generating an electromagnetic (EM) field. Rapid shutoff of the current generates eddy currents in the conductive body (the earth), which generate a time-varying secondary electromagnetic field. This is measured by the receiver coil through diffusive induction (Schamper et al., 2013). Raw data from tTEM surveys is in the form of the time derivative of the magnetic flux passing through the receiver coil, dB/dt, of the survey instrument. These measurements can be used to estimate the electrical resistivity of subsurface

materials through an inversion process. Variations in resistivity can indicate the presence of sand, bedrock, and confining clay layers that influence groundwater flow.

2.2 Field Campaign

2.2.1 tTEM Surveys

Electromagnetic data were collected with the tTEM at the study site in March, May, June, August, and September 2024. Table 2 shows the dates of data collection and the types of data collected.

Table 2: Survey dates and data collected. All dates are listed in mm/dd/yyyy format.

Survey Date	Data Collected
03/22/2024	tTEM, near-surface soil volumetric water content
05/16/2024	tTEM, near-surface soil volumetric water content
06/27/2024	tTEM, near-surface soil volumetric water content
08/07/2024	tTEM, near-surface soil volumetric water content
09/19/2024	tTEM, near-surface soil volumetric water content, water conductivity

Time between the first two surveys was dependent on equipment repairs. Beginning in May, surveys were spaced approximately six weeks apart. Initial survey path lines were located approximately 30 m apart. Surveys were conducted along path lines as close as possible to previous survey paths, but some variation occurred due to the study site's irregular field shape, uneven terrain, and limited precision and timely location updates of the GPS system used to track survey paths. Figure 5 shows a map of the study site and tTEM survey path lines from all five surveys.

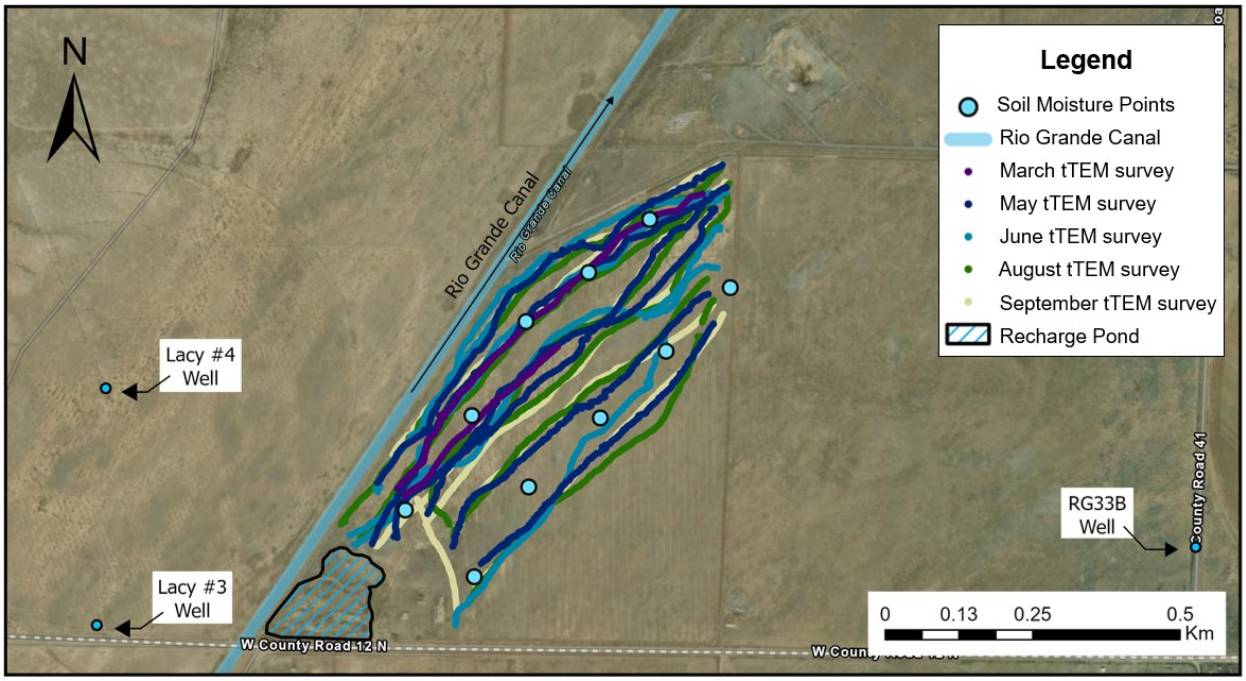

Figure 5: Map of surveyed area showing the locations of tTEM path lines and soil moisture measurements. Imagery source: ESRI World Imagery.

Path lines were approximately parallel to the Rio Grande Canal, which was used to convey irrigation water to on-farm turnouts in the area from April to November 2024. This configuration was selected partly to detect changes in saturation across parallel profiles and partly based on field layout and the large turning radius of the tTEM system. Path lines perpendicular to the Rio Grande Canal would have been necessarily shorter and further from the canal due to the turning radius of the system.

2.2.2 Other Measurements

Soil water content, electrical conductivity, and temperature were measured conjunctively with tTEM surveys in 10 locations at the study site using a Stevens Water Hydraprobe handheld soil sensor. While the shallow (6 cm) depth of measurements precluded direct comparison to tTEM measurements, which cover a larger scale of depth at lower resolution, they provide a

useful reference for seasonal trends in near-surface soil water content. Water samples from the Rio Grande Canal, four other nearby canals, and a nearby well were collected in September 2024 to measure the conductivity of water present in the system. Additional data used to analyze results include canal flow measurements from the Colorado Department of Natural Resources gage 2000812 (Rio Grande Canal Near Del Norte, RIOCANCO), precipitation data from the Colorado Climate Center, lithology data from well logs, and well water level measurements from the Rio Grande Water Conservation District. Figure 5 shows the locations of soil water content point measurements at 6 cm depth, the locations of wells that were used for water level measurements and referencing lithology data, the recharge pond, and the Rio Grande Canal. Flow in the canal runs from southwest to northeast. The tTEM surveys covered an area of approximately 40 hectares.

2.3 Data Processing

Noise can be introduced in TEM data from mechanical vibrations and rotations while driving over rough terrain, as well as power lines and other sources of EM signals (Schamper et al., 2013). High-pulse repetition frequency of measurements allowed random noise from surveys to be canceled out in raw stacks, and final time gate values were obtained by stacking, as described by Auken et al. (2019). A low-pass filter in the AGS Workbench software package was used to suppress motion-induced noise in the data.

2.3.1 Inversion

The inverse problem addresses the need to find a model of the earth that is consistent with the observed data. The model can be validated with existing geologic information. tTEM data were processed and inverted using the 1D forward model in AGS Workbench. Raw dB/dt

data were filtered manually to remove electrical and mechanical noise. Laterally constrained inversions (LCI), using a 40 ohm-m homogeneous half-space as an initial model, were performed for all datasets. In a laterally constrained inversion, the solution is forced to adhere to spatial relationships between points on either side (Santos 2004; Auken et al., 2005). This ensures lateral consistency to result in a more geologically realistic solution. Workbench utilizes the AarhusInv inversion code. The resistivity model was discretized between 30 layers with fixed layer boundaries. The regularization process penalized vertical changes in resistivity using an L2 (smooth) norm to produce a vertically smooth resistivity model (Seequent 2025).

2.3.2 Interpolation

Following the inversion of full datasets in AGS Workbench, resulting resistivity data were interpolated using empirical Bayesian kriging in ArcGIS Pro. The empirical Bayesian method automatically calculates kriging parameters for a dataset through a process of subsetting and simulations; data are divided into subsets, and semivariogram parameters are estimated for each subset using restricted maximum likelihood (REML), rather than weighted least squares used in other kriging methods. This method accounts for the uncertainty in estimating semivariogram model parameters, which results in greater accuracy of standard errors of prediction. Other kriging methods may underestimate standard errors of prediction due to their assumption that an estimated semivariogram is the true semivariogram for the data (ESRI 2025). Semivariograms for each subset are plotted together, and predictions in a given location are calculated from the simulated semivariograms in the subsets covering the search neighborhood for the location. This method has been shown to be advantageous for interpolating datasets with moderately nonstationary data because it uses an intrinsic random function as the kriging model

(Krivoruchko and Gribov, 2019). Correcting for trends in the data was appropriate in this study due to the spatial variability of resistivity values.

K-Bessel semivariogram models were selected for all five datasets to minimize the standard error of prediction and provide the best fit between empirical semivariances and the median distribution of semivariograms. Semivariograms for each dataset are shown in Appendix B. Table 3 shows semivariogram parameters used in kriging models for each resistivity dataset. The default number of simulations (100) was used for all datasets.

Table 3: Semivariogram statistics for empirical Bayesian kriging models.

Dataset	Standardized RMS	Average Standard Error
March 2024	0.92	2.98
May 2024	0.57	3.49
June 2024	0.64	4.41
August 2024	0.65	9.02
September 2024	0.72	11.2

A single line running parallel to the Rio Grande Canal, selected for its proximity to path lines from all five surveys, was demarcated and populated with kriged resistivity values using a nearest neighbor approach. This process was repeated for a line running perpendicular to the canal that bisected path lines from all five surveys. Isolating data from transect lines enabled direct comparison of subsurface resistivity at the study site from month to month.

3. RESULTS

3.1 Field Measurements

Repeating surveys in the exact same location following the initial March survey was hindered by uneven field topography and a lag in the GPS display used for orientation in the field. Other variations in spatial coverage of survey path lines resulted from variable field conditions including weather and limitations in available daylight during time in the field. Mean depth of investigation (DOI) for the tTEM surveys ranged from 83-117 m bgs, with an overall mean of 97 m bgs, based on the conservative DOI values calculated in AGS Workbench. Figure A2 in Appendix A shows the distribution of DOI values across the five tTEM surveys. The DOI is estimated by recalculating the Jacobian matrix of the final inverted model and applying a threshold value based on the minimum amount of sensitivity required (Christiansen and Auken, 2012). At depths exceeding the DOI, the signal to noise ratio increases sufficiently to cause the inversion to converge back to the starting resistivity model.

Figure 6 shows a cross-sectional view of the Rio Grande Canal and the area surveyed by the tTEM.

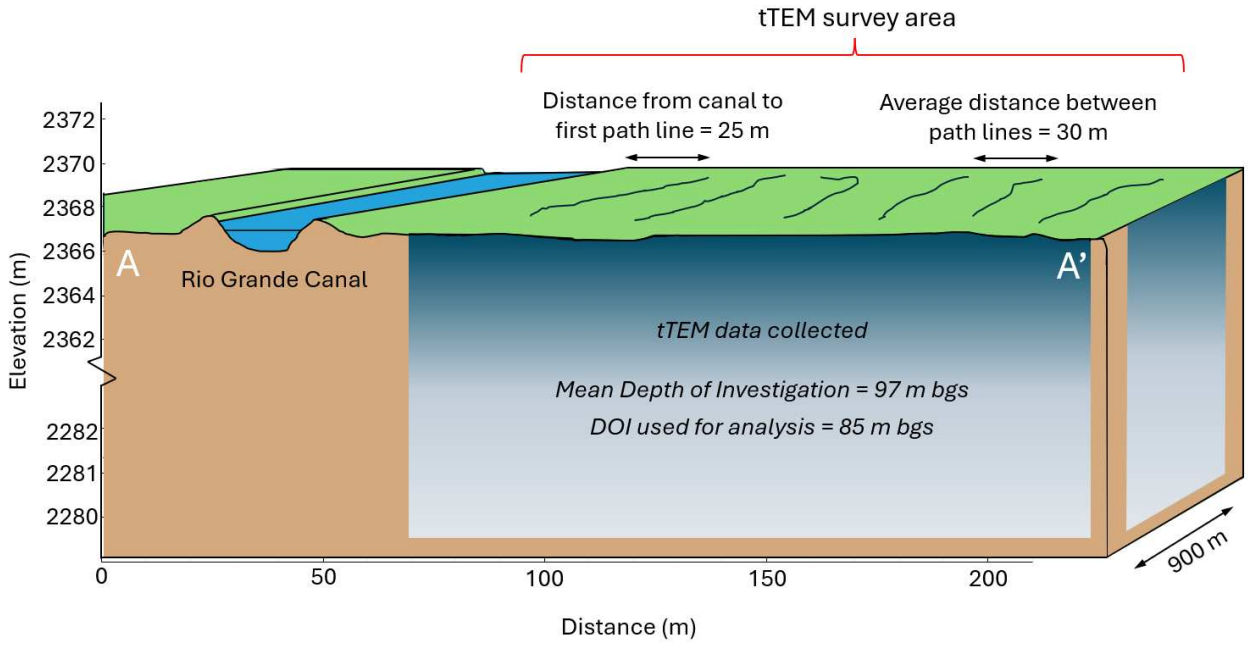

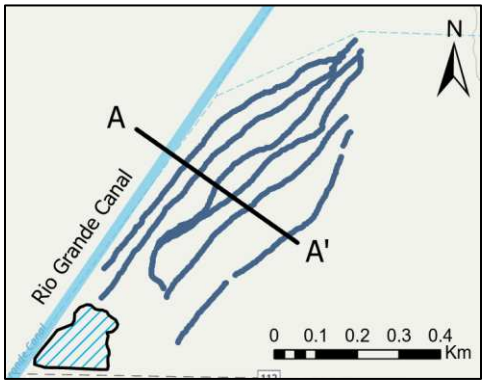

Figure 6: *Above:* Cross-sectional view of Rio Grande Canal and surveyed area. Elevations showing the topography of the upper 2m of the subsurface are to scale based on 1-m lidar data for the site (USGS 2020). *Left:* Plan view map showing the location of transect A-A' used for cross section. Path lines from the August tTEM survey are shown for reference.

3.1.1 Observed Soil Water Content

Figure 7 shows the seasonal trend in soil volumetric water content. Average near-surface soil volumetric water content of approximately 13% moisture was observed in March, followed by an increase to approximately 17% moisture in the May survey. Average soil volumetric water content decreased to approximately 6% and 4% moisture in measurements from June and August, respectively, and increased to approximately 13.2% moisture in the measurement in September following precipitation events earlier in the month.

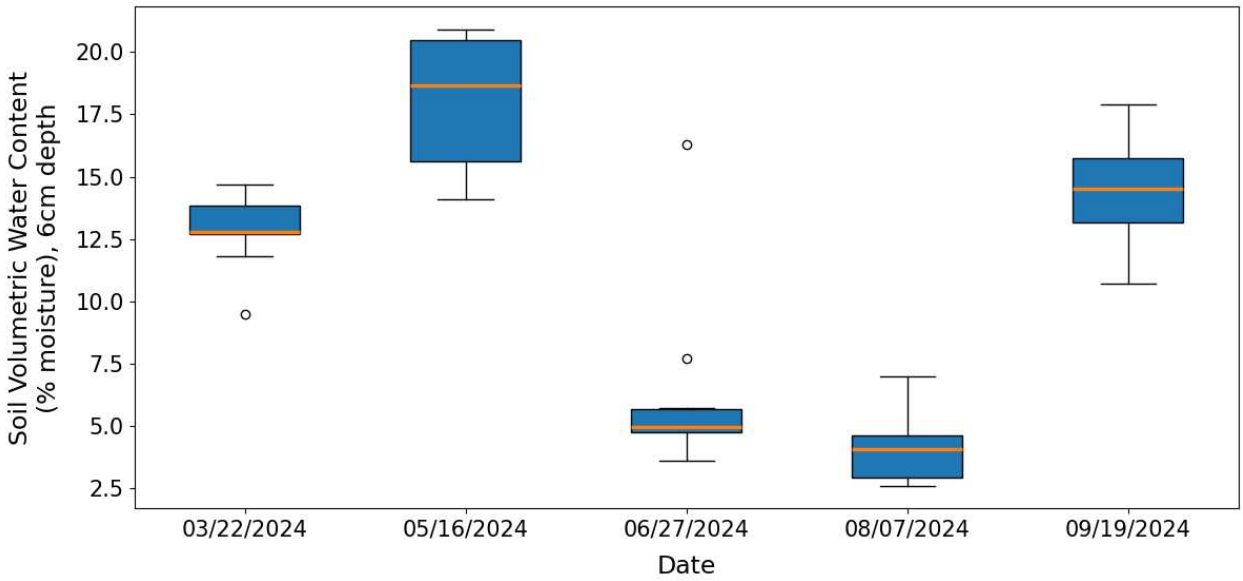

Figure 7: Seasonal soil volumetric water content distributions across point measurements.

The soil excavated during soil water content sampling was observed to be silty, sandy, and contained many rounded rocks. This is consistent with descriptions of the regional lithology in well logs and in previous studies of the area (Siebenthal 1910; Lipman 1976; Sunada et al., 1983; Harmon 2020).

3.1.2 Canal Flow and Precipitation

Figure 8 shows flow in the Rio Grande Canal and precipitation. The dates of tTEM surveys are indicated by dashed red lines. Canal flow data were obtained from the Colorado Department of Natural Resources gage 2000812 (Rio Grande Canal Near Del Norte, RIOCANCO). This gage is located directly downstream of the diversion for the Rio Grande Canal and is approximately 11 kilometers southwest of the study site. Precipitation data were obtained from the Colorado Climate Center's Del Norte 3ENE weather station (station ID 052184), located in Del Norte, Colorado, approximately 7.5 kilometers southwest of the study site.

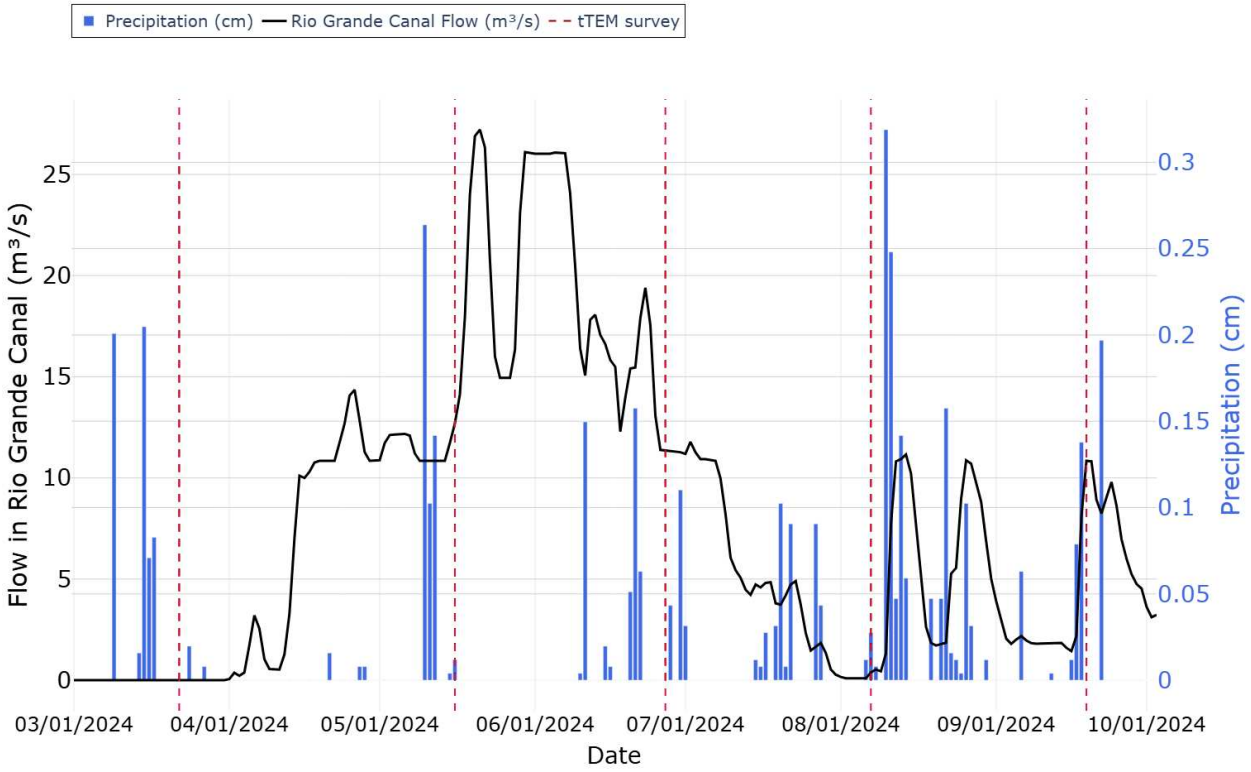

Figure 8: Gaged flow in the Rio Grande Canal and precipitation.

Flow changes can be seen in the Rio Grande Canal in response to precipitation. The amount of water released to the canal is dependent on the gage height of the Rio Grande River, leading precipitation events to have an impact on canal flow through both direct contributions to the canal and through impacts to the gage height in the Rio Grande River. Flow in the canal is also influenced by the timing and volume of calls made by water rights holders for water deliveries. The second tTEM survey, conducted in mid-May 2024, had high volumetric water content in the upper soil, and a prolonged period of seepage from canal flow. Precipitation was also highest leading up to this survey date. The tTEM survey in early August 2024 corresponded to the lowest volumetric water content, as well as low precipitation and no canal flow preceding

the survey. In addition to the data presented here, this trend was observed qualitatively during field surveys.

3.1.3 Water Levels in Wells

Figure 9 shows the observed water levels in three wells adjacent to the survey site. The RG33B well, located to the southeast of the area surveyed with the tTEM, had a pressure transducer that logged daily measurements of water level. Water levels in the Lacy #3 well, located to the southwest of the area surveyed with the tTEM, were measured monthly using a manual water level meter. The Lacy #4 well, located to the west of the area surveyed with the tTEM, had a pressure transducer logging daily water level measurements, but the sensor was not installed until August 7, 2024. Water level measurements from the Lacy #4 well were not available prior to that date.

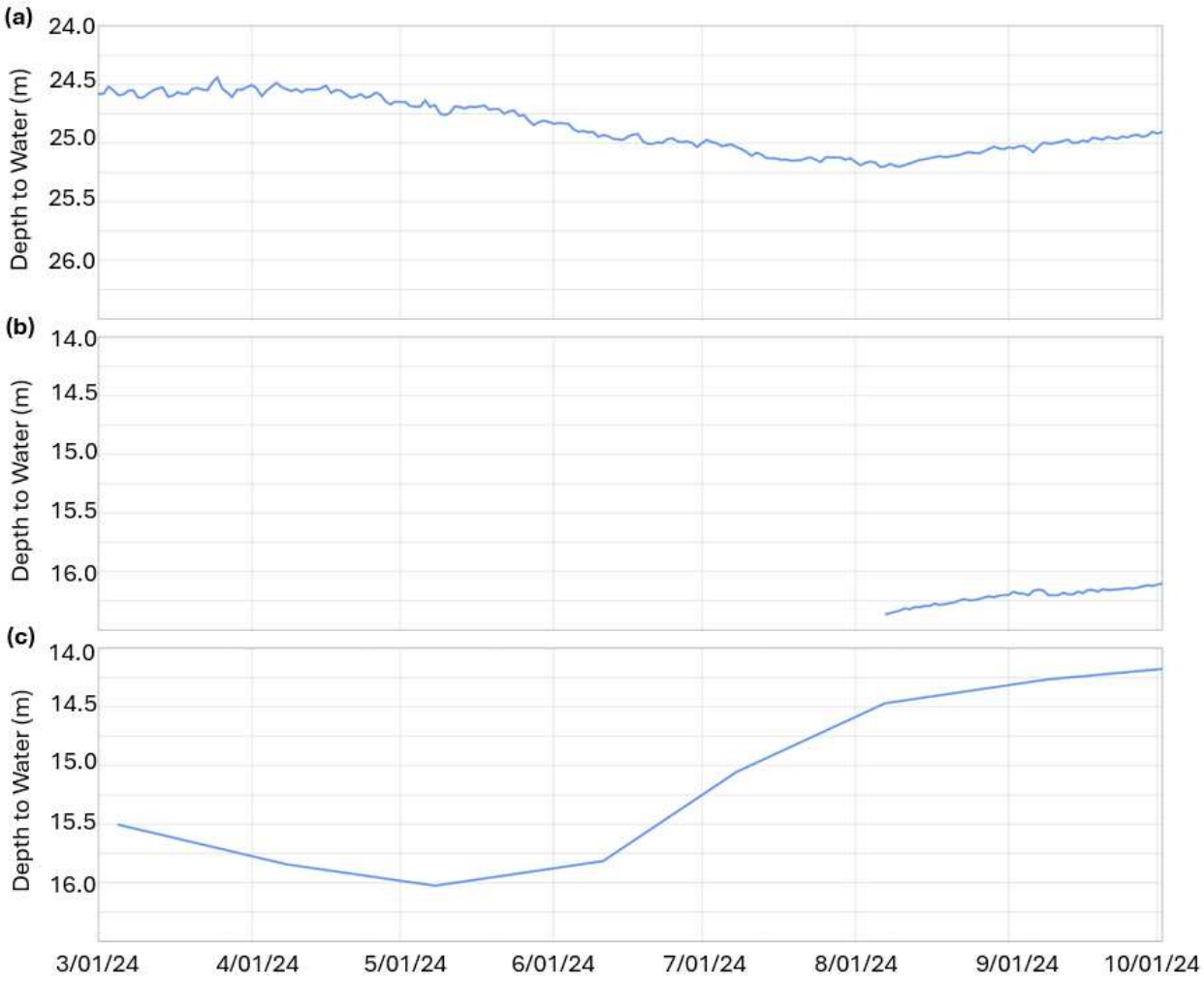

Figure 9: Depth to water (m bgs) in (a) RG33B, (b) Lacy #3, and (c) Lacy #4 wells.

As shown in Figure 9, water levels in the three wells ranged from approximately 14 to 25.25 m bgs throughout the season. Water levels in the RG33B and Lacy#4 wells changed by less than 1 m throughout the season. In the Lacy #3 well, the water level changed by approximately 2 m across the season. Water level trends in all three wells were positive from August to October. The water level trend in Lacy #3 was positive following the May measurement, which contrasts to the trend seen in the RG33B well, which was negative from April to August.

Figure B6 in Appendix B shows interpolated groundwater levels based on monitoring well data collected in September 2024. Interpolation was completed using ordinary kriging with a Gaussian variogram model. The results shown in Figure B6 represent an estimate of the regional water table, independent of the effects of managed recharge.

3.1.4 Water Quality Samples

Table 7 in Appendix C shows the resistivity (converted from conductivity) of water samples from various sources of surface water used for recharge, and a nearby well, in September 2024. Surface water sampled from five canals in the area, including the Rio Grande Canal, had an average resistivity of 188 ohm-m. A single sample from the Rio Grande Canal had a resistivity of 178 ohm-m. Water sampled from a well approximately 0.25 km from the tTEM survey area had a resistivity of 139 ohm-m. These results are summarized in Table 7 in Appendix C.

3.2 Post-Processing Results

3.2.1 Resistivity Models

Figure 10 shows a three-dimensional view of the resistivity model developed from the May tTEM survey data.

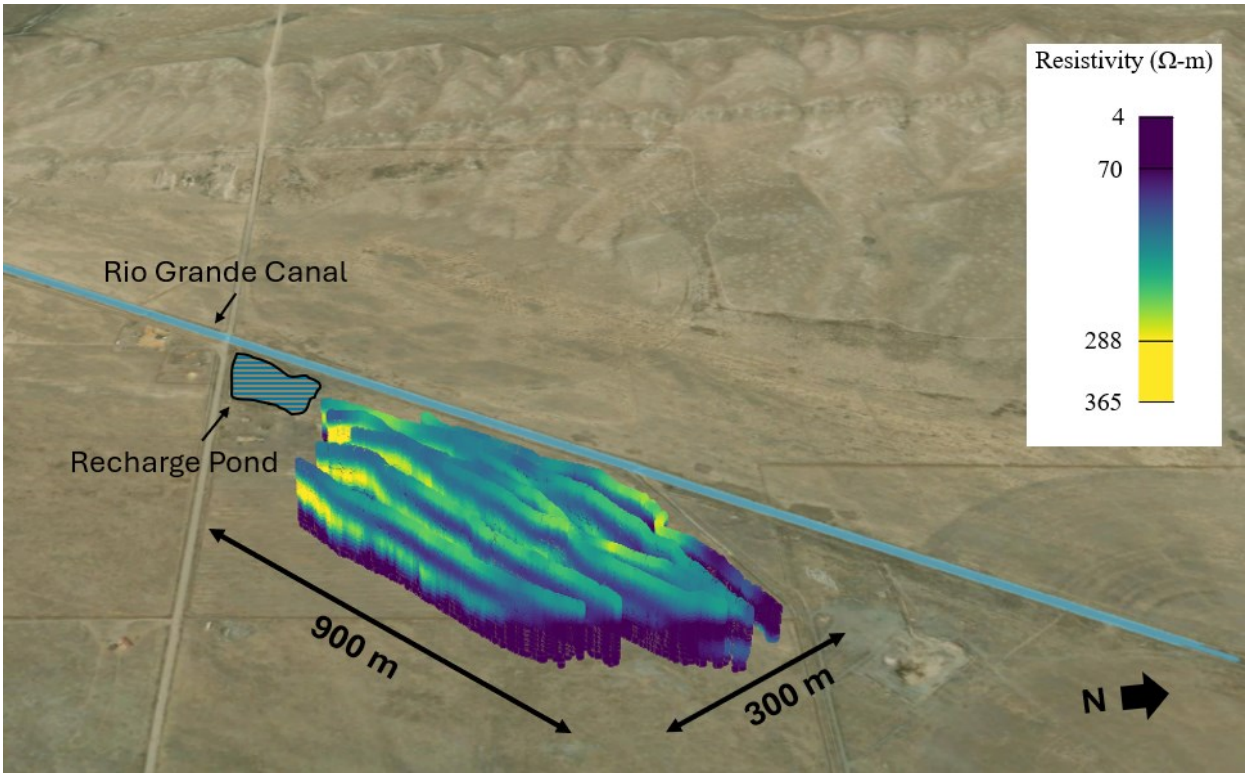

Figure 10: Three-dimension view of resistivity model from the acquired data in May. Imagery source: ESRI World Imagery.

Figure 11 shows a map of the study site with the locations of tTEM soundings and the transect lines used for profile plots. Transects were located parallel and perpendicular to the canal to provide a comparison of resistivity profiles over time.

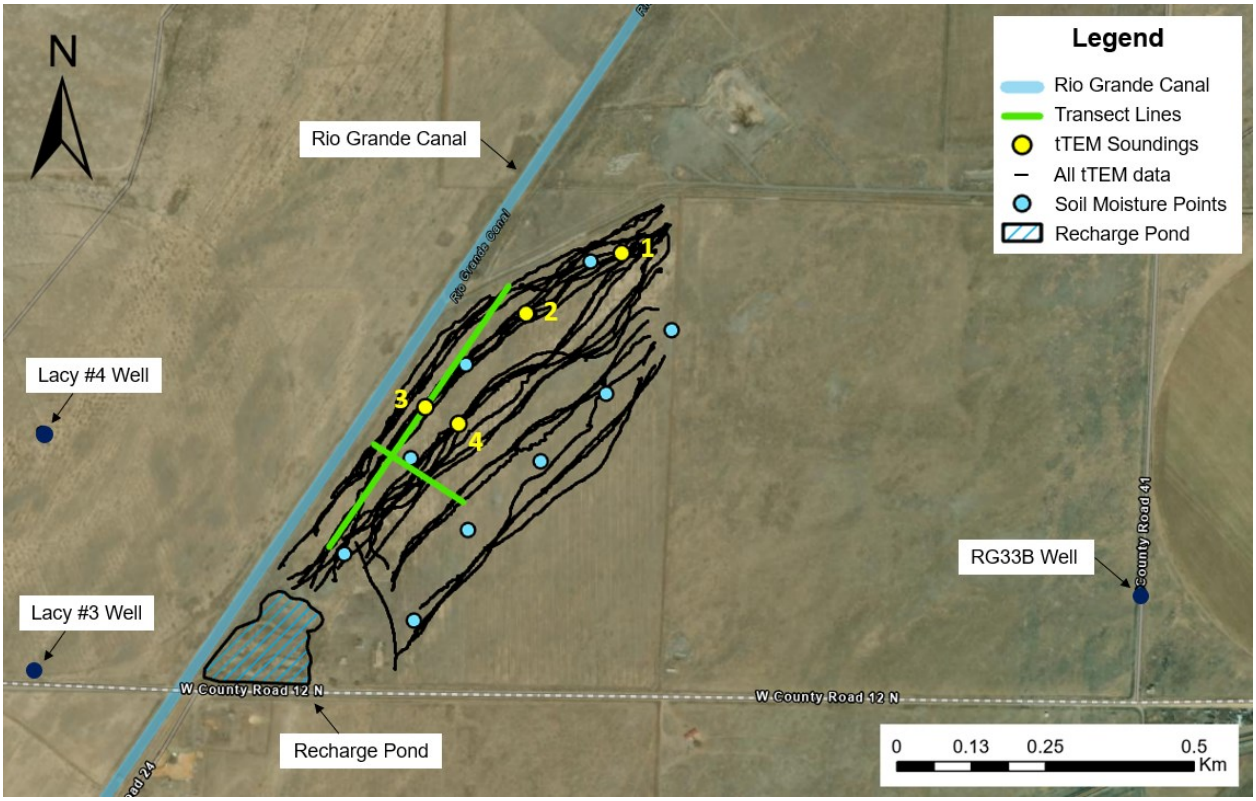

Figure 11: Map of study site, tTEM survey locations, soundings shown in individual plots, and transect lines used for profile plots. Soundings are labeled 1-4. Imagery source: ESRI World Imagery.

Figure A3 in Appendix A shows the distribution of resistivity values from tTEM surveys. The values were limited to data within an area covered by all five surveys. This area is shown in Figure A4 in Appendix A. Figure 12 shows resistivity with depth for a single tTEM sounding selected across datasets ("sounding 1"). Figures A5, A6, and A7 in Appendix A show resistivity with depth for soundings 2, 3, and 4. The locations of selected soundings are indicated in yellow in Figure 11. Soundings from each dataset were selected as close as possible to one another, with a maximum separation distance of 15 m. The blue dashed line indicates the estimated depth of the water table in March 2024. The depth of the water table, estimated based on water level measurements from wells and modeled resistivity, fluctuated over the course of the season.

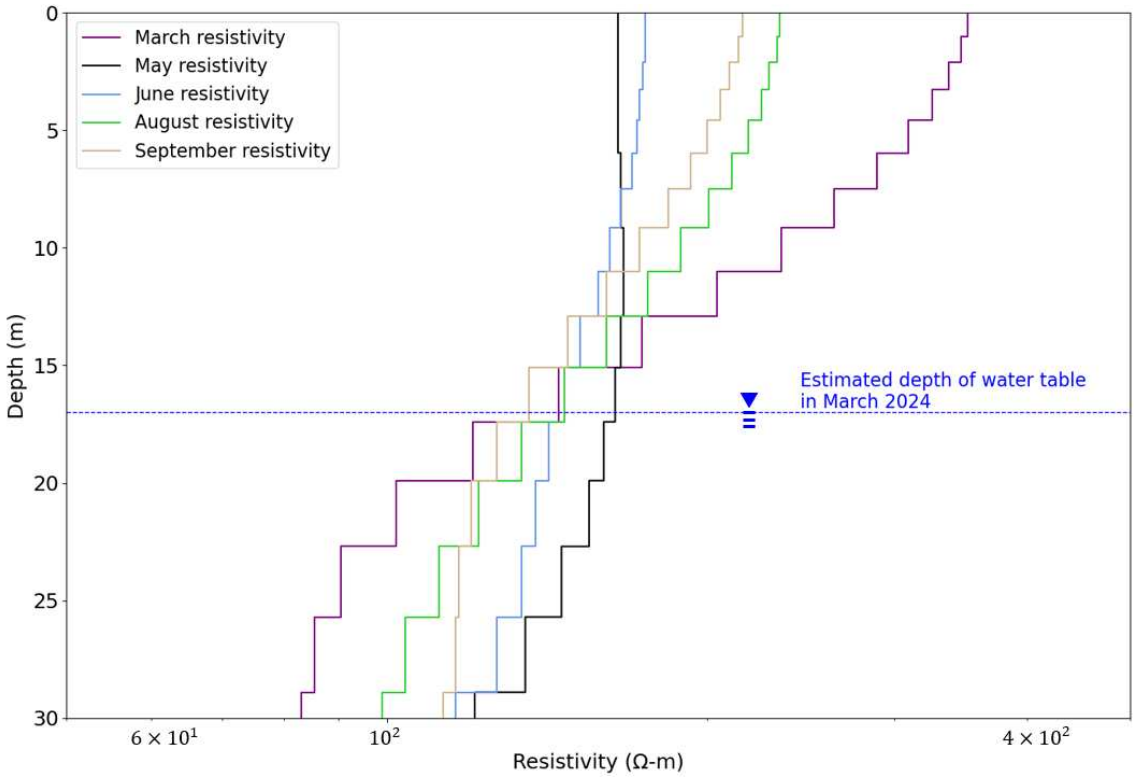

Figure 12: resistivity values from Workbench inversion compared to estimated depth of water table at sounding 1.

3.2.2 Interpolation Results

Figure 13 shows resistivity values from inverted data across all survey months for a transect parallel to the canal, while Figure 14 shows resistivity values for a transect perpendicular to the canal. Data were acquired using 3-dimensional empirical Bayesian kriging and a nearest neighbor approach from the transect lines shown in green in the map in Figure 11. Depths shown are below the ground surface, which is approximately 2367 m above mean sea level (variations in ground surface elevation are not shown; in the profile plots, a depth of 0 m corresponds to an elevation of approximately 2367 m, which is the maximum elevation in the interpolated datasets within the threshold used to acquire values along transect lines). The dashed line in each plot indicates the estimated location of the water table based on modeled resistivity.

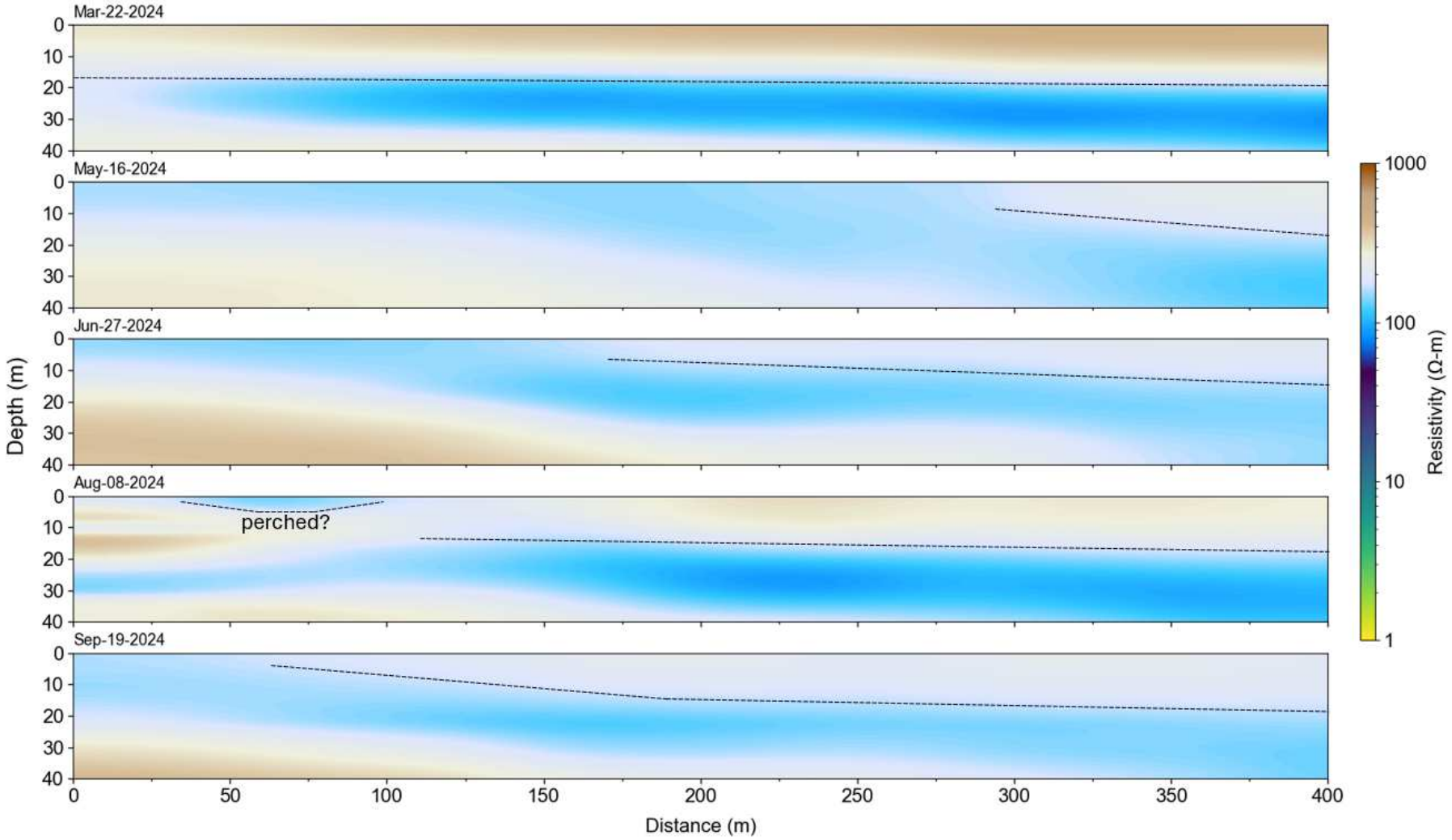

Figure 13: Resistivity profiles for each month along transect parallel to Rio Grande Canal. Distance increments along the transect go from southwest to northeast. The location of the parallel transect is shown in Figure 11. The dashed lines indicate the estimated location of the water table.

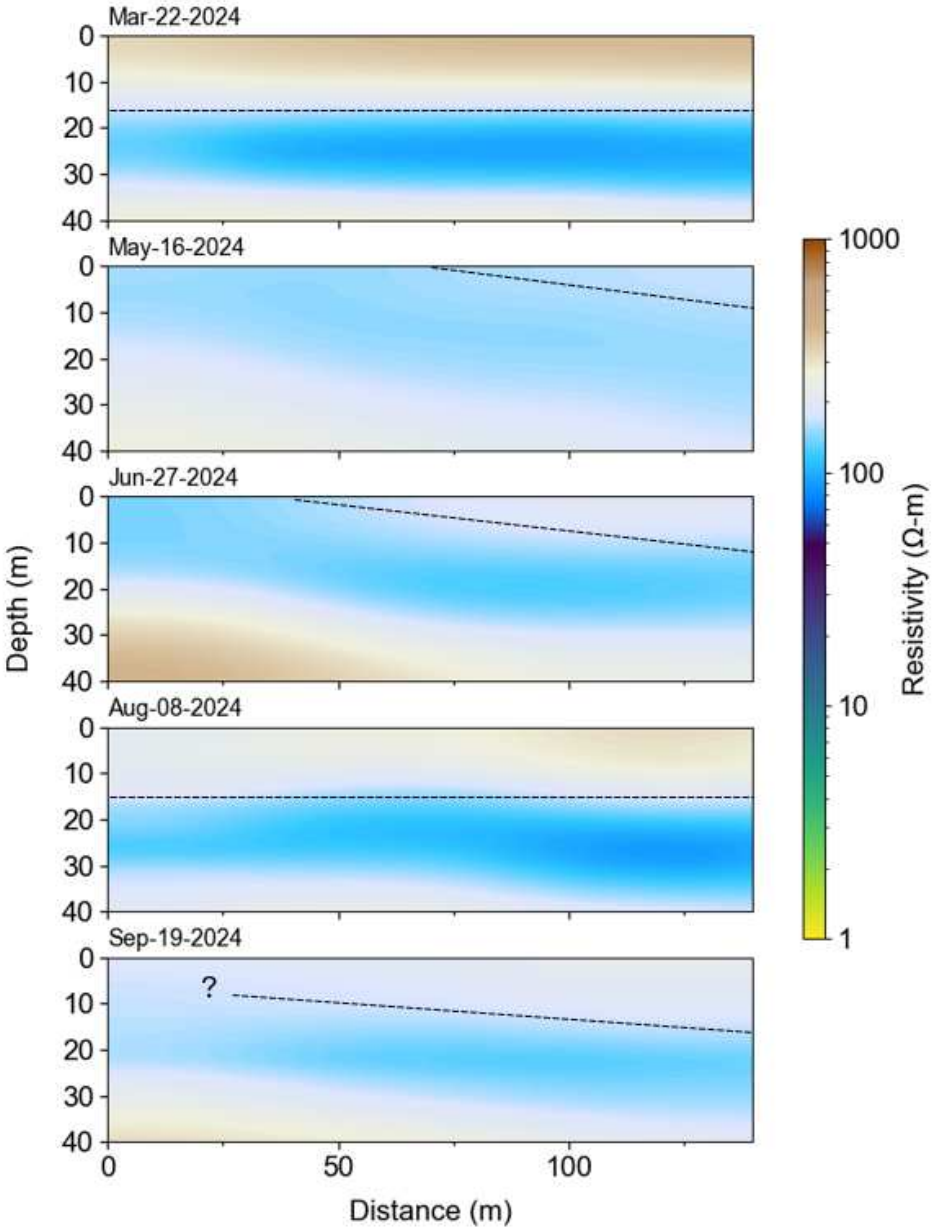

Figure 14: Resistivity profiles for each month along transect perpendicular to Rio Grande Canal. Distance increments along the transect go from northwest to southeast, increasing in distance away from the canal. The location of the perpendicular transect is shown in Figure 11. The dashed lines indicate the estimated location of the water table.

Changes in resistivity across survey datasets vary by depth. Resistivity in the upper 17-20 m of the subsurface follows a trend similar to the variation in near-surface soil water content measurements, with relatively high resistivity (corresponding to dry conditions) in March transitioning to lower resistivity in May. An increase in resistivity in the upper 17-20 m of the subsurface was observed from June to August, and from August to September the resistivity in this area decreased.

4. DISCUSSION

4.1 Changes in Resistivity

4.1.1 Factors Affecting Subsurface Resistivity

Subsurface resistivity is primarily a function of lithology and saturation. The effects of soil structure on resistivity remain constant with time, so it was assumed that differences in resistivity between repeated measurements could be attributed primarily to changes in saturation. Nevertheless, other factors have the potential to influence subsurface resistivity. Pore fluid salinity and total dissolved solids (TDS) were assumed to have limited effects on changes in resistivity through the duration of the study, as both have been observed at low levels in the region. Groundwater salinity in the boundary of the valley-fill deposits, where the study site is located, has been observed in low to medium concentrations, which are defined as having a specific conductance less than 250 µmho and between 250-750 µmho, respectively (Edelmann and Buckles, 1984). The concentration of TDS in groundwater is low to moderate in most parts of the valley, with the exception of the sump area in the north-central part of the valley (Barkmann et al., 2020). The specific conductance of groundwater in the region was not expected to change over the duration of the study in quantities that would make it a dominant driver of changes in resistivity. It is possible, however, that pore fluid composition (i.e., ion concentration) had some effect on changes in resistivity over the course of the season. As shown in Table 7 in Appendix C, a notable difference was observed in resistivity of surface water in the Rio Grande Canal and groundwater extracted from a nearby well (178 ohm-m vs. 139 ohm-m, respectively). Conductivity measurements were made in September, when it is expected that groundwater resistivity would be relatively high compared to other parts of the year due to recharge from the canal and pond over the preceding months. While expected to be minor

compared to the effects of saturation, the effects of seasonal changes in water chemistry could have some effect on changes in resistivity, particularly below the regional water table, where saturation did not change over the course of the study period.

Changes in the temperature of soil and pore fluids, while assumed to be present over the study duration, cannot be corrected for directly in resistivity data due to a lack of direct temperature measurements at the site. The effects of temperature fluctuations on TEM measurements can be estimated, however, through quantification of uncertainty. Campbell et al. (1948) found a conductivity increase of approximately 2% per °C between 15 and 35 °C. This finding was supported in later work by Colman and Hendrix (1949) and Schlumberger (1989). Temperature changes are relevant for the upper 1 m of the subsurface but considered negligible at depths greater than 4 m (Singh and Sharma, 2017). In addition, resistivity observations did not follow the trend expected with higher temperatures (i.e., higher temperatures in August corresponded with higher resistivity values in the upper 15 m of the subsurface). For the purposes of this study, inverted resistivity values above the March water table were interpreted as indications of changes in saturation for the identification of seasonal trends.

4.1.2 Observed Changes in Resistivity

Clear changes in subsurface resistivity were observed from March through September. In the upper 17-20 m of the subsurface, resistivity was relatively high in March and decreased in May and June. Increases in resistivity in the upper 17-20 m of the subsurface were observed in August, followed by decreases in September. These changes in resistivity in the unsaturated zone correspond to the timing of flows in the canal and precipitation events and are interpreted as being driven by changes in saturation. The increases in saturation are likely influenced primarily

by seepage from the canal and the recharge pond. Infiltration in the vadose zone is controlled by various factors, including the initial saturation levels of sediments, lithologic structure, hydraulic heads in the aquifer system (which are dynamic and influenced by activities elsewhere in the system), and hydraulic heads of the water applied, in the case of surface recharge methods. Recharge from precipitation was not expected to penetrate to depths in quantities large enough to detect through resistivity changes due to the limited quantity and frequency of precipitation events, and the scale and resolution of tTEM measurements.

Resistivity values observed in the upper 17-20 m (interpreted as the region above the water table) at the study site in March 2024 indicate that the water table near the canal is very similar to regional water table measurements. This is consistent with the observation that no canal or recharge pond seepage had occurred up to that point in the season, so the water table was likely not strongly influenced by managed recharge. Between March and May 2024, the site likely underwent a phase of initial wetting, and recharge flow behavior may have changed throughout this phase as primary flow conduits, or preferential flow paths in the unsaturated zone, were filled. Changes in resistivity in the unsaturated zone (upper 17-20 m) suggest that the effects of recharge were highly localized in the study time frame. The estimated location of the water table, shown by the dashed lines in Figure 13 and Figure 14, rose near the surface in May, and appeared to have a gradient moving downward from southwest to northeast along the parallel transect line shown in Figure 11. In June, the water table in the parallel transect appeared to have a similar, albeit less steep, downward gradient. In August the gradient flattened out more, and there appeared to be a perched water table between approximately 30 and 100 m down the transect line. A perched water table can be expected in this location due to its proximity to the recharge pond and the otherwise dry conditions (lack of active recharge) in early August, which

could lead to reduced head and the accumulation of recharge water behind lower-permeability sediments. In September, the water table is estimated to rise again due to increased recharge, again showing a downward gradient from southwest to northeast along the parallel transect (Figure 13).

Head gradients in the system dictate the direction of flow, as demonstrated by the downward slant in the water table moving away from the canal and pond. Along the perpendicular transect, the groundwater table was estimated to slant downward away from the canal and pond in months where recharge was active or had been occurring (i.e., May, June, and September), while under conditions of little to no recharge (March and August) the water table appeared to have minimal gradient and be located at greater depths.

Water level measurements from wells indicate the location of the water table at well locations ranged between 14-16.5 m bgs on the west side of the canal, and between 24.25 and 25.25 m bgs east of the canal, through the duration of the study. Between those depths and the ground surface, sediments remained unsaturated, with varying levels of soil water content. In the area between point measurements from wells, tTEM observations coupled with known recharge efforts suggest that the location of the water table fluctuated significantly throughout the study duration, as described above. A clear relationship was observed between the timing of recharge and changes in resistivity, indicating the effects of recharge on subsurface saturation and demonstrating the capability of time-lapse tTEM measurements for detecting groundwater recharge dynamics.

Changes in resistivity were also observed below the water table. In the saturated zone, these changes are interpreted as resulting partially from the constraints used in the inversion process (e.g., smoothing and fixed layer thicknesses; see Figure 12 in Knight et al., 2018, for an

example of how inverted resistivity can vary from true resistivity values based on the constraints and model type used in the inversion). A more accurate characterization of resistivity, particularly in the region below the water table, could be achieved with a time-lapse inversion strategy customized to better capture time-varying changes.

Due to the high head gradients shown in Figures 13 and 14, as well as the high hydraulic conductivity in the study area indicated by the presence of coarse materials in drillers' logs and indicated by high resistivity measurements, rapid movement of water from the canal to the aquifer is likely. Resistivity measurements below the regional water table in Figure 12 provide some support for this mechanism, as the water was most conductive in March, prior to managed aquifer recharge efforts began that season. Managed recharge likely decreased the concentration of total dissolved solids in the groundwater in later months. Thus, differences in the chemistry of recharge water and in-situ groundwater are another factor that could have contributed to changes in resistivity below the water table. The estimated location of the water table in March in the locations of tTEM surveys (Figure 12, Figures A5-A7) indicates that some areas in the saturated zone had relatively high (>150 ohm-m) resistivity, in some places exceeding the resistivity of the groundwater (the average resistivity of canal water, based on measurements in September, was 188 ohm-m, while the resistivity of water sampled from a nearby well was 139 ohm-m; Table 7 in Appendix C details the observed resistivity values of water samples). The bulk resistivity of lithologic units with higher intrinsic resistivity is more sensitive to fluctuations in water chemistry. Thus, we consider higher-resistivity water entering the subsurface from the canal and pond, along with uncertainty in the inversion model, to be possible contributors to the changing resistivity values observed from month to month in the saturated zone shown in Figure 13 and Figure 14.

4.2 Lithology Interpretation

This study corroborates previously existing understanding of the local geology in the study area, while providing insight into field-scale characteristics of the study location and west-central region of the SLV. Previous studies (Siebenthal 1910, Lipman 1976, Sunada et al., 1983, Harmon 2020) have described the lithology in the west-central edge of the San Luis Valley as characterized by coarse- to medium-grained alluvial deposits. Despite agreement on regional geological characteristics among previous studies, little was known about the specific geology of the site prior to this study. Well logs for the RG33B, Lacy #3, Lacy #4, and other wells in the vicinity contain sparse descriptions of lithology; all describe sand and gravel-dominated materials, with limited exceptions in the form of thin (<2 m) clay layers. Well logs for the RG33B and Lacy #4 wells, and the well permit for Lacy #3 (for which a drillers log was not available) are contained in Appendix D. The distinction between varying subsurface materials is critical for recharge site assessment, as minor variations in hydraulic conductivity caused by differences in sand composition or the presence of thin clay lenses can be sufficient to render managed recharge activities unsuccessful. Resistivity values from tTEM surveys at the study site correspond to primarily sandy and silty materials. While these results are consistent with descriptions of regional geological features found in previous work, site-specific information about the locations of low- and high-resistivity materials provides necessary insight for understanding recharge mechanisms and can contribute to the design of targeted recharge facilities, particularly in locations where barriers to recharge (i.e., low-K zones) exist).

4.2.1 Relationship Between Resistivity, Porosity, and Saturation

Higher resistivities observed in the saturated zone can be attributed to clean sands (i.e., sands that are free of clay minerals or shale) based on an analysis of the measured conductivity of recharge water and resistivity data, as demonstrated in the application of Archie's law (1942). Archie's law, shown in Eq. (1), relates the resistivity of a porous rock (ρ_0) to its pore water resistivity (ρ_f), porosity ϕ, and saturation, S (the fraction of the voids filled with water):

$$\rho_0 = \alpha \rho_f \phi^{-m} S^{-n} \quad (1)$$

In this equation, the cementation exponent m, tortuosity coefficient α, and saturation exponent n are site-specific material constants. This equation is considered valid for medium to coarse-grained soils and rocks and operates under the assumption that the soil material does not contribute to electrical conductivity (Frohlich and Parke, 1989). Table 4 shows calculation results for resistivities corresponding to various soil types using Eq. (1). Full calculations used to estimate the soil type based on resistivity data are shown in Appendix C.

Table 4: Calculated resistivity values with corresponding porosity and soil types. Average values for porosity and resistivity are show in parentheses.

Soil Type	Porosity Range (%)	Calculated Resistivity (ohm-m) (saturated conditions)	Calculated Resistivity (ohm-m) (unsaturated conditions)
Gravel	25-44 (35)	202-421 (277)	20,200-42,000 (27,700)
Coarse sand	31-46 (39)	191-319 (240)	19,100-32,000 (24,000)
Fine sand	25-53 (39)	159-421 (236)	15,900-42,000 (23,600)

Based on the collected tTEM data, information from well logs in the vicinity, and common ranges of resistivity values for various soil materials, the lithologies were interpreted as shown in Figure 15. This interpretation characterizes the site as having a predominantly sandy

lithology. Some saturated regions have resistivities much higher than those of saturated clays (see Appendix C), but lower than resistivities indicated by Table 4 that would be expected for a clean sand, where Eq. (1) is valid. These regions are thus assumed to have some conductive material and are interpreted as silty sands.

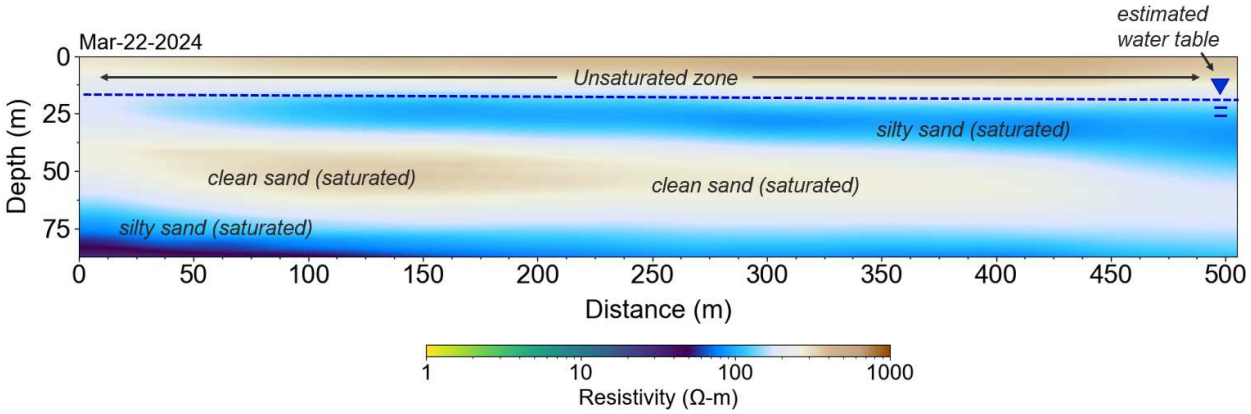

Figure 15: Interpretation of site lithology based on tTEM data and information from nearby well logs. Cross section is the same parallel transect from March 2024 shown in Figure 13.

Table 11 in Appendix C shows resistivity values for common soil types, including the soils shown in Figure 15. Resistivity of saturated sands is usually greater than 22 ohm-m, while the resistivity of saturated clays typically falls in the range of 1-12 ohm-m (Anthony 2006; Knight et al., 2018; Li et al., 2024). While some silt is likely present in the areas surveyed, the ranges of resistivities in the inverted data suggest that the fraction of silty materials is sufficiently small to classify sediments in the area surveyed as sands (and thus enable the application of Archie's law).

4.2.2 Conceptual Model of Hydrogeology

A conceptual model of the hydrogeology of the study site was developed based on tTEM survey results, well water level measurements in September, and lithology descriptions from available well logs in the area. This is shown in Figure 16(b). Figure 16(a) shows the locations of the wells and transects shown in the conceptual diagram.

(a)

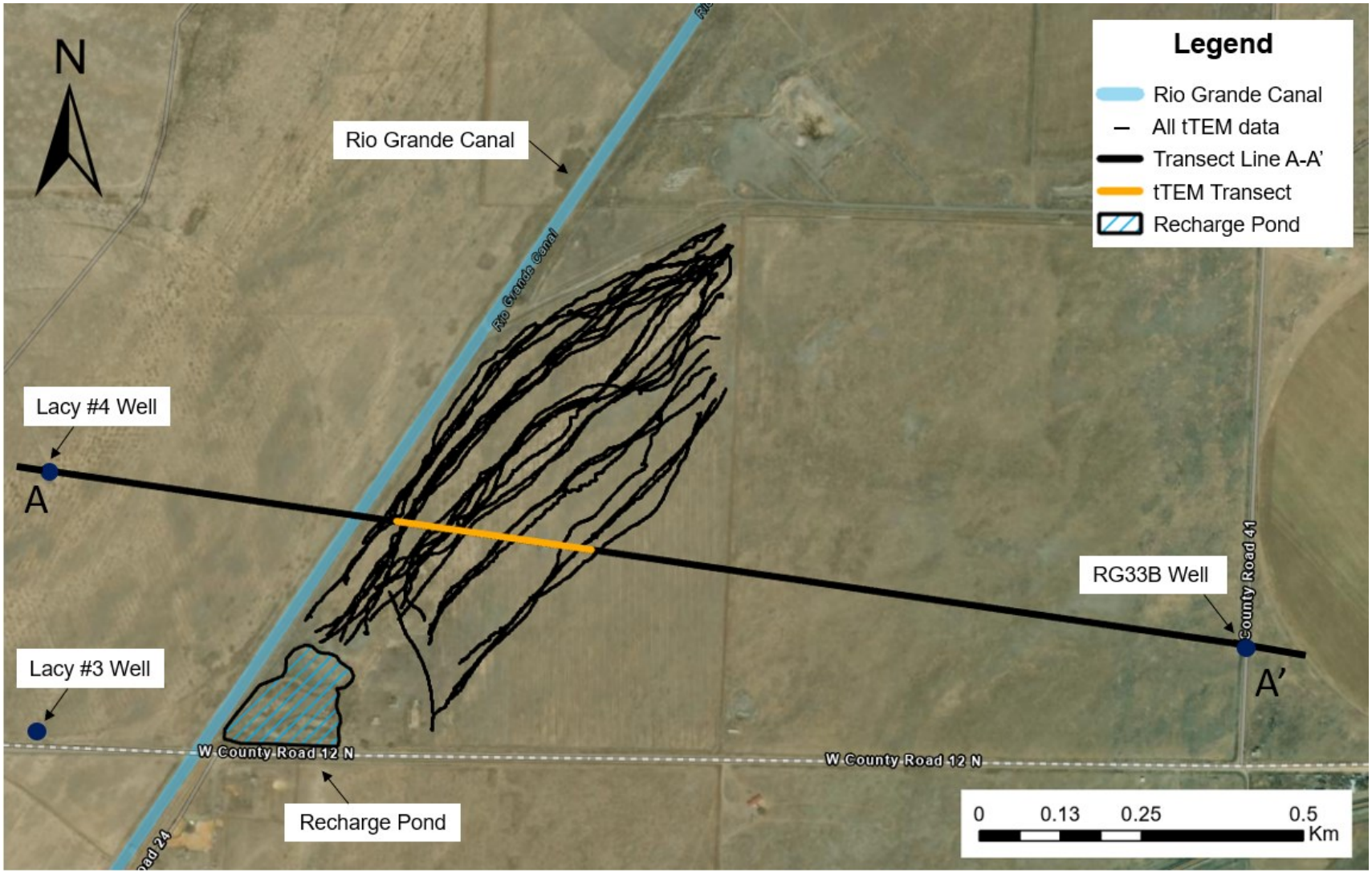

Figure 16(a): Site map showing locations of wells and transects shown in conceptual diagram. The transect in orange shows the location of the tTEM data profile shown in Figure 16(b).

(b)

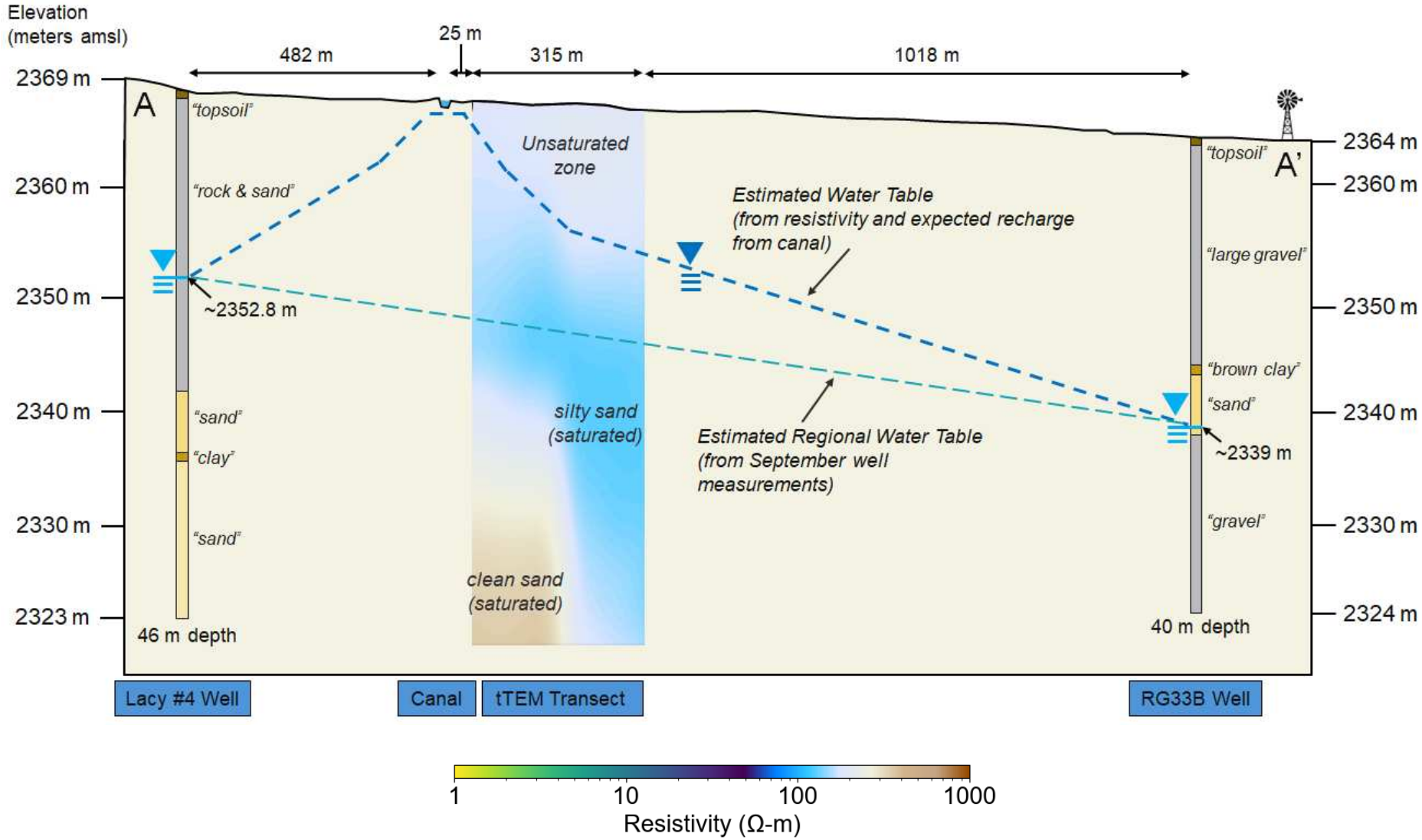

Figure 16(b): Conceptual model of hydrogeology at the study site, transect A-A'. Lithology notes in quotations are based on descriptions from corresponding well logs. Water levels in wells are from measurements in September 2024. Elevations showing surface topography are to scale based on 1-m lidar data for the site (USGS 2020).

Despite the regional homogeneity described in studies of the western edge of the San Luis Valley, the drivers of site-specific variations in water levels measured in wells, and the specific flow pathways of recharge water applied to the study area, were not well understood prior to this study. Figure 16(b) provides insight into recharge dynamics at the study site.

Differences in water level measurements from wells, without considering the tTEM data or the influence of the canal and recharge pond, indicate an east-by-northeast trending horizontal hydraulic gradient. This gradient is likely not linear, however, due to seepage from the canal and recharge pond, which are both located in between the aforementioned wells. Resistivity cross-sections shown in Figure 13 and Figure 14 show zones of lower resistivity adjacent to the canal and recharge pond at times following applications of recharge water. The water table locations shown in Figure 14 also indicate a horizontal hydraulic gradient moving away from the locations of recharge; this indicates a clear response in saturation levels from sources of recharge.

Water levels in the Lacy #3 and RG33B wells follow opposing trends from May to August (Figure 9). Declines in water level in the RG33B well were likely driven by pumping from irrigation wells supplying center pivot systems to the east of the well; the number of wells in operation in the 2024 season increases as one moves east from the study site. The Lacy #3 well is located farther away from active irrigation wells and is closer to the canal and recharge pond at the study site Increases in water level in the Lacy #3 and Lacy #4 wells correspond to times of active recharge and can be attributed to seepage from the Rio Grande Canal and the recharge pond. The Lacy #3 and Lacy #4 wells were likely affected by pumping to a lesser degree than the RG33B well given their distance from irrigation wells that were actively in use.

The water level data from nearby wells are limited by low spatial resolution, and in the case of the Lacy #3 well, low temporal sampling. The wells used for water level measurements

have screened lengths up to 22 m, which introduces uncertainty in measurements due to the potential for vertical gradients leading to cascading in the wells. Vertical gradients are unlikely in this region, however, due to the lack of extensive clays. Given this and the absence of other points of reference, these measurements are useful for estimating the location of the regional water table throughout the duration of the study. It was assumed that the top of the saturated zone was equivalent to the water table elevation. This assumption is not valid if a capillary fringe layer exists (Dewar and Knight 2020) but was considered acceptable in this study due to the dominance of coarse-grained sediments, which have a very small capillary fringe. Based on an interpolation of measurements from nearby wells alone, the water table was observed to fluctuate between approximately 17-20 m bgs in the area surveyed with the tTEM. However, with the additional data acquired from tTEM, we estimate that during periods of active recharge, the depth to the water table ranged from the ground surface near the canal to 17-20 m bgs at a distance of approximately 450 m from the canal, while during periods of no recharge, the water table near the canal was similar to the regional water table.

4.2.3 Assessment of Site Suitability for Managed Recharge

The effects of configuration of subsurface geologic facies on the groundwater recharge response is an important factor to consider in the assessment of MAR sites. In alluvial aquifer systems where semi-confining layers exist, the aquifer response to recharge can vary widely depending on the geologic structure. Given sufficient hydraulic connection between a recharge site and the aquifer, recharge can result in both local increases in groundwater storage and the possibility of a more widespread increase in pressures in the regional aquifer system (Maples et al., 2019). This consideration is less critical for the western edge of the San Luis Valley, where semi-confining layers are less common compared to the central and eastern parts of the valley. In

any case, it is important to distinguish between local and regional responses to recharge, as they have different impacts on water rights and water policy issues (Maples et al., 2019).

Based on the site-specific resistivity data and estimated lithology detailed in the preceding discussion, the study site is a good fit for managed recharge, with few barriers to infiltration. The first 200 m of the transect line parallel to the canal shown in Figure 11 is expected to have a higher K compared to the other parts of the transect due to the decreases in observed resistivity in that area following recharge events; however, that area's proximity to the canal and recharge pond limits this interpretation. Pepin et al. (2022) describe the depth to the shallowest no-flow unit and the lengths of preferential flow paths as key factors affecting recharge site suitability. By that metric, the absence of field-scale confining layers and low tortuosity observed in resistivity cross-sections make the study site a suitable location for managed recharge.

4.3 Use of tTEM for Time-Lapse Studies

The successful processing and utilization of tTEM from repeat surveys can enable larger-scale, more rapid time-lapse geophysical studies to answer hydrologic questions and inform groundwater management, including tools like managed aquifer recharge. This study serves as a baseline assessment for direct comparison of resistivity datasets acquired through individual, laterally constrained inversions. Spatial differences between acquisitions are a key barrier to implementing time-constrained inversions commonly used in time-lapse geophysical studies (Singha et al., 2015); the use of empirical Bayesian kriging enabled comparison between non-collocated datasets after data had been inverted with lateral constraints. The workflow outlined in this study is well-suited for providing data with relatively low computational requirements to

assess changes in subsurface resistivity over time, addressing a need for efficient assessment of subsurface characteristics on a field scale.

4.3.1 Inversion and Interpretation of Resistivity

Differences in model regularization may have contributed to observed changes in resistivity. Regularization parameters are a particularly important factor to consider when comparing datasets from separate surveys and separate inversions. To investigate this, the raw data were examined prior to inversion. Figure A1 in Appendix A shows raw data plotted for all survey datasets for four points, which were selected based on their proximity to one another amongst all five datasets (the locations of these points are shown in Figure 11). These plots show similar results for raw data soundings between surveys, which could be indicative of the presence of inversion artifacts. However, observed changes in resistivity between datasets are sufficiently large to suggest that changes were driven by factors in addition to potential inversion artifacts (e.g., changes in saturation resulting from recharge). In the upper 17-20 m of the subsurface (unsaturated zone), where saturation levels are expected to fluctuate the most, a clear correlation was observed between the volume of water in the canal and changes in resistivity. Saturation levels were likely the primary driver of observed changes in resistivity in the unsaturated zone; resistivity changes can be attributed to either a rising water table or increased vadose zone saturation in the upper 17-20 m. The degree of changes observed in resistivity between datasets, and the agreement observed qualitatively between changes in resistivity and the timing of recharge at the study location, warrant the use of the aforementioned results for providing assessments of trends in groundwater infiltration at the study site, in spite of uncertainties stemming from the inversion.

In any electromagnetic method, the EM field is diffusive and produces a measurement averaged over a volume rather than at a single point or depth (Christiansen et al., 2016). This is another assumption and potential limitation to consider in the interpretation of inversion results. Interpretations of inversion results cannot be made based on changes in resistivity observed in single points at depth so much as trends observed over larger spatial extents. Regularization settings used in inversions should favor the smallest model variation consistent with the data to avoid misrepresentation of physical processes in the inversion model.

Recharge volume is another important consideration in the interpretation of resistivity data for understanding recharge processes; the ability of electromagnetic methods to detect a wetting front can be limited in cases with low volumes of infiltrating water. In a field scale setting, given the non-uniqueness of inversion methods for TEM soundings, it is possible for the range of uncertainty in modelled resistivity values to exceed the resistivity variation caused by natural changes in moisture content (Binley et al., 2002). The volume of seepage entering the aquifer from the Rio Grande Canal and the recharge pond at the study site was assumed to be large enough to detect through modelled resistivity, despite the uncertainty of the inversion, but this potential variability must be considered, among other sources of uncertainty. Changes in resistivity observed throughout the season corresponded to the timing of flows in the Rio Grande Canal and water deliveries to the recharge pond, which supports this assumption.

5. CONCLUSIONS

An improved understanding of groundwater recharge processes can benefit stakeholders in the San Luis Valley and other arid and semi-arid regions that depend on groundwater. Direct-sampling methods of groundwater monitoring (e.g., drilling) are often cost-prohibitive and do not provide data on sufficient spatial and temporal scales to adequately inform regional water management decision-making. Geophysical methods like time-domain electromagnetic surveys can address the need for cost-effective, high-resolution hydrostratigraphic data collection with greater spatial and temporal coverage in locations where recharge and groundwater flow processes are poorly understood.

This study took a novel approach to using the tTEM system for time-lapse geophysical measurements, enabling more rapid data acquisition at greater depths of investigation and at larger scales than other geophysical methods. A key challenge of using tTEM for time-lapse studies is in the integration of survey datasets covering different line paths. This challenge was addressed through the use of empirical Bayesian kriging, which enabled direct comparison of geophysical datasets from separate acquisitions. A strong correlation was observed between volume of recharge water and changes in resistivity at the study site, indicating time-varying changes in vadose zone saturation and informing estimates of the depth to the water table. With few exceptions, resistivity data from the study site were consistent with properties of high-K, coarse-grained sediments, demonstrating the suitability of the study site as a location for managed recharge. Results from this study demonstrate the ability of mobile TEM surveys to resolve seasonal changes in subsurface resistivity through time-lapse measurements. This technique can be used to improve siting and design of groundwater recharge sites, among other

applications, serving as an important tool for addressing groundwater depletion and contributing to more sustainable groundwater management and use.

6. REFERENCES

Anthony, E. (2006). Groundwater Exploration and Management using Geophysics: Northern Region of Ghana. Univ. Cottbus, 156 S. S., DOI: https://doi.org/10.23689/fidgeo-340.

Archie, G. E. (1942). The Electrical Resistivity Log as an Aid in Determining Some Reservoir Characteristics. http://onepetro.org/TRANS/article-pdf/146/01/54/2179020/spe-942054-g.pdf/1

Auken, E., A.V. Christiansen, L. Jacobsen, & K. I. Sørensen (2005). Laterally constrained 1D inversion of 3DTEM data: Symposium on the Application of Geophysics to Engineering and Environmental Problems（SAGEEP）Proceedings, 519–524.

Auken, E., Foged, N., Larsen, J. J., Lassen, K. V. T., Maurya, P. K., Dath, S. M., & Eiskjær, T. T. (2019). tTEM - A towed transient electromagnetic system for detailed 3D imaging of the top 70 m of the subsurface. *Geophysics*, *84*(1), E13–E22. https://doi.org/10.1190/geo2018-0355.1

Ball, L. B., Bloss, B. R., Bedrosian, P. A., Grauch, V. J. S., & Smith, B. D. (2015). *Airborne Electromagnetic and Magnetic Survey Data of the Paradox and San Luis Valleys, Colorado*. U.S. Geological Survey Open-File Report 2015-1024. http://dx.doi.org/10.3133/ofr20151024.

Barkmann, Peter E., Lauren D. Broes, Martin J. Palkovic, John C. Hopkins, Kenneth Swift Bird, Lesley A. Sebol, and F. Scot Fitzgerald. "ON-010 Colorado Groundwater Atlas." Geohydrology. Colorado Geological Survey, Golden, CO. ON-010 Colorado Groundwater Atlas, 08 January 2020. https://coloradogeologicalsurvey.org/water/colorado-groundwater-atlas/

Beetle-Moorcroft, F., Shanafield, M., & Singha, K. (2021). Exploring conceptual models of infiltration and groundwater recharge on an intermittent river: The role of geologic controls. *Journal of Hydrology: Regional Studies*, *35*, 100814. https://doi.org/10.1016/J.EJRH.2021.100814

Behroozmand, A. A., Auken, E., & Knight, R. (2019). Assessment of Managed Aquifer Recharge Sites Using a New Geophysical Imaging Method. *Vadose Zone Journal*, *18*(1), 1–13. https://doi.org/10.2136/vzj2018.10.0184

Bexfield, L.M., & S.K. Anderholm (2010). Section 10.-Conceptual Understanding and Groundwater Quality of the Basin-Fill Aquifer in the San Luis Valley, Colorado and New Mexico, in Thiros, S.A., Bexfield, L.M., Anning, D.W., and J.M. Huntington, eds., Conceptual Understanding and Groundwater Quality of Selected Basin-Fill Aquifers in the Southwestern United States. U.S. Geological Survey Professional Paper 1781, pp. 165-172.

Bianchi, M., Zheng, C., Tick, G.R. and Gorelick, S.M. (2011). Investigation of Small-Scale Preferential Flow with a Forced-Gradient Tracer Test. Groundwater, 49: 503-514. https://doi.org/10.1111/j.1745-6584.2010.00746.x

Campbell, R.B., Bower, C.A., & L.A. Richards (1948). Change of electrical conductivity with temperature and the relation of osmotic pressure to electrical conductivity and ion concentration for soil extracts. Soil Sci. Soc. Proc. 66–69.

Chen, K., J. Zhang, G. Xue, H. Huang, W. Chen, J. Hao, and Y. Yue. (2019). Feasibility of monitoring hydraulic connections between aquifers using time-lapse TEM: A case history in Inner Mongolia, China: Journal of Environmental and Engineering Geophysics, 24, 361–372. https://doi.org/10.2113/JEEG24.3.361

Christiansen, A.V., & Auken, E. (2012). A global measure for depth of investigation. *Geophysics*, *77*(4). https://doi.org/10.1190/geo2011-0393.1

Christiansen, A.V., J.B. Pedersen, E. Auken, N.E. Søe, M.K. Holst, and S.M. Kristiansen (2016). Improved geoarchaeological mapping with electromagnetic induction instruments from dedicated processing and inversion. Remote Sens. 8(12):1022. doi:10.3390/rs8121022

Colman, E.A., & T.M. Hendrix (1949). The fiberglass electrical soil-moisture instrument. Soil Sci. 67, 425–438.

Colorado Water Conservation Board (2025). Colorado Department of Natural Resources. Interstate Compacts: Rio Grande Compact. https://dnrweblink.state.co.us/CWCB/0/edoc/211608/Art66Title37.pdf?

Dewar, N., & Knight, R. (2020). Estimation of the top of the saturated zone from airborne electromagnetic data. *Geophysics*, *85*(5), EN63–EN76. https://doi.org/10.1190/geo2019-0539.1

Edelmann, P. & D.R. Buckles (1984). Quality of Ground Water in Agricultural Areas of the San Luis Valley, South-Central Colorado. U.S. Geological Survey Water-Resources Investigations Report 83-4281. Lakewood, Colorado.

El-Kaliouby, H., T. Ferré, and K. Zonge (2007). Examination of the potential for time domain electromagnetic method for monitoring infiltration and recharge in arid areas: Journal of King Abdulaziz University-Earth Sciences, 18,71–87, doi: 10.4197/Ear.18-1.4.

ESRI (2019). What is empirical Bayesian kriging? ArcGIS Pro Help. https://pro.arcgis.com/en/pro-app/latest/help/analysis/geostatistical-analyst/what-is-empirical-bayesian-kriging-.htm

Fitterman, D. v., & Grauch, V. J. S. (2010). Transient Electromagnetic Mapping of Clay Units in the San Luis Valley, Colorado. *Proceedings of the Symposium on the Application of Geophyics to Engineering and Environmental Problems, SAGEEP*, *1*, 154–164. https://doi.org/10.4133/1.3445428

Freeze, R.A. and Cherry, J.A. (1979). Groundwater. Prentice-Hall Inc., Englewood Cliffs, Vol. 7632, pp. 38-46.

Frohlich, R. K., & Parke, C. D. (1989). The Electrical Resistivity of the Vadose Zone — Field Survey. *Groundwater*, *27*(4), 524–530. https://doi.org/10.1111/j.1745-6584.1989.tb01973.x

Garba, M. A., Vialle, S., Madadi, M., Gurevich, B., and M. Lebedev, M. (2019). Electrical formation factor of clean sand from laboratory measurements and digital rock physics. Solid Earth, 10, 1505–1517, https://doi.org/10.5194/se-10-1505-2019.

Harmon, E. J. (2020). Groundwater Resources of Colorado's San Luis Basin. In J. M. Beeton, C. N. Saenz, and B. J. Waddell (Eds.), *The Geology, Ecology, and Human History of the San Luis Valley*. (pp. 183-207). University Press of Colorado, Louisville, Colorado. https://doi.org/10.5876/9781646420407

Hawley, J., and M. Kernodle. 2000."Overview of the Hydrogeology and Geohydrology of the Northern Rio Grande Basin—Colorado, New Mexico, and Texas." In *Proceedings of the 44th Annual New Mexico Water Conference*, ed. C. T. Ortega Klett, 79–102. Socorro: New Mexico Water Resources Research Institute.

Heagy, L., Cockett, R., Kang, S., Rosenkjaer, G., & D. Oldenburg. (2017). A framework for simulation and inversion in electromagnetics. Computers & Geosciences, Volume 107, 2017, Pages 1-19, ISSN 0098-3004, http://dx.doi.org/10.1016/j.cageo.2017.06.018.

HRS Water Consultants, Inc. (2002). RGDSS Final Memorandum: Ground Water Task 32—Hydrogeologic Database Refresh. Denver: Colorado Division of Water Resources.

Haoping Huang, H. & A. Cogbill (2006). Repeatability study of helicopter-borne electromagnetic data. Geophysics. 71: G285-G290. https://doi.org/10.1190/1.2353797

Huntley, D. (1979). Ground-water recharge to the aquifers of northern San Luis Valley, Colorado: Geological Society of America Bulletin, Part II, v. 90, no. 8, p. 1196–1281.

Keller, G. R., Cordell, L., Davis, G. H., Peeples, W. J., & White, G. (1984). *A geophysical study of the San Luis Basin*. 51–57. In *Rio Grande Rift (Northern New Mexico).* https://doi.org/10.56577/ffc-35.51

King, J., T. Mulder, G. O. Essink, & M. F. P. Bierkens. (2022). Joint estimation of groundwater salinity and hydrogeological parameters using variable-density groundwater flow, salt transport modelling and airborne electromagnetic surveys. Advances in Water Resources, 160, 104118. doi: 10.1016/j.advwatres.2021.104118.

Knight, R., Smith, R., Asch, T., Abraham, J., Cannia, J., Viezzoli, A., & Fogg, G. (2018). Mapping Aquifer Systems with Airborne Electromagnetics in the Central Valley of California. *Groundwater*, *56*(6), 893–908. https://doi.org/10.1111/gwat.12656

Krivoruchko K. and Gribov A. (2019). "Evaluation of empirical Bayesian kriging," *Spatial Statistics* Volume 32. https://doi.org/10.1016/j.spasta.2019.100368.

Kuenhold, O.J. (2004). Concerning the matter of the rules governing new withdrawals of ground water in water division no. 3 affecting the rate or direction of movement of water in the confined aquifer system aka "confined aquifer new use rules for division 3". District Court, Water Division No. 3, Colorado Alamosa County Courthouse, 702 Fourth Street, Alamosa, Colorado 81101.

Li, J., Smith, R., Grote, K., & Pedersen, J. B. (2024). Aquifer characterization using towed time-domain electromagnetics in a variably saturated, data-sparse region. *Journal of Applied Geophysics*, *228*. https://doi.org/10.1016/j.jappgeo.2024.105440

Lipman, P.W. (1976). Geologic map of the Del Norte area, eastern San Juan Mountains, Colorado. 10.3133/i952. USGS Publications Warehouse. https://pubs.usgs.gov/publication/i952

Loke, M.H., Chambers, J.E., Rucker, D.F., Kuras, O., Wilkinson, P.B. (2013). Recent Developments in the direct-current geoelectrical imaging method. J. Appl. Geophys. 93: 135-156. http://dx.doi.org/10.1016/j.jappgeo.2013.02.017

Markovich, K. H., Manning, A. H., Condon, L. E., & McIntosh, J. C. (2019). Mountain-Block Recharge: A Review of Current Understanding. In *Water Resources Research* (Vol. 55, Issue 11, pp. 8278–8304). Blackwell Publishing Ltd. https://doi.org/10.1029/2019WR025676

Maurya, P. K., Christiansen, A. V., Pedersen, J., & Auken, E. (2020). High resolution 3D subsurface mapping using a towed transient electromagnetic system - tTEM: case studies. *Near Surface Geophysics*, *18*(3), 249–259. https://doi.org/10.1002/nsg.12094.

McLachlan, P., Christiensen, N.B., Grombacher, D. & Christiansen, A.V. (2023) Evaluating the impact of correlated noise for time-lapse transient electromagnetic (TEM) monitoring studies. *Near Surface Geophysics*, 21, 333–342. **https://doi.org/10.1002/nsg.12262**

Palacky, G.J. (1987). 3. Resistivity Characteristics of Geologic Targets. *Investigations in Geophysics*: 52-129. https://doi.org/10.1190/1.9781560802631.ch3

Pepin, K., Knight, R., Goebel-Szenher, M., & Kang, S. (2022). Managed aquifer recharge site assessment with electromagnetic imaging: Identification of recharge flow paths. *Vadose Zone Journal*, *21*(3). https://doi.org/10.1002/vzj2.20192

Phillips, R. (2021). Restoring Aquifers and Dealing With Drought at the San Luis Valley Irrigation District. Irrigation Leader, 24 (3), March 2021: Severe Drought on the Rio Grande. Water Strategies, LLC, Washington, DC.

Reynolds, J.M. (2011). An Introduction to Applied and Environmental Geophysics. 2nd Edition, John Wiley and Sons Ltd., New York, p. 291.

RGWCD (Rio Grande Water Conservation District) (2024). Special Improvement District No. 1 of the Rio Grande Water Conservation District: Annual Replacement Plan, 2024 Plan Year. Rio Grande Water Conservation District, Alamosa, Colorado.

Samouëlian, A., Cousin, I., Tabbagh, A., Bruand, A., & Richard, G. (2005). Electrical resistivity survey in soil science: A review. In *Soil and Tillage Research* (Vol. 83, Issue 2, pp. 173–193). https://doi.org/10.1016/j.still.2004.10.004

Santos, F. A. M. (2004). 1-D laterally constrained inversion of EM34 profiling data: Journal of Applied Geophysics, 56, pp. 123–134.

Schamper, C., Pedersen, J. B., Auken, E., Christiansen, A. v., Vittecoq, B., Deparis, J., Jaouen, T., Lacquement, F., Nehlig, P., Perrin, J., & Reninger, P. A. (2013). Airborne Transient EM Methods and Their Applications for Coastal Groundwater Investigations. In *Coastal Research Library* (Vol. 7, pp. 121–153). Springer. https://doi.org/10.1007/978-94-007-5648-9_7

Schlumberger (1989). Log Interpretation Principles and Application. Schlumberger Educational Services, Houston, SMP-7017.

Seequent (2025). AarhusInv inversion code. https://www.seequent.com/products-solutions/ags-workbench/aarhusinv-inversion-code/

Siebenthal, C.E., 1910, The San Luis Valley, Colorado: Science, new series, v. 31, p. 744-746.

Simpson, C. (2018). A Tale of Two Rivers: Groundwater Management in the South Platte & Rio Grande Basins. Adams State University, 17 September 2018, Alamosa, CO, United States.

Singh, R.K. and R.V. Sharma (2017). Numerical analysis for ground temperature variation. *Geotherm Energy* **5**, 22. https://doi.org/10.1186/s40517-017-0082-z

Singha K., Day-Lewis F. D., Johnson T., & Slater L. D. (2015), Advances in interpretation of subsurface processes with time-lapse electrical imaging, *Hydrol. Process.*, 29; pp. 1549–1576, doi: 10.1002/hyp.10280

Slater L & Binley A. (2021). Advancing hydrological process understanding from long-term resistivity monitoring systems. *WIREs Water*. 2021; 8:e1513. https://doi.org/10.1002/wat2.1513

Sunada, D.K., Warner, J.W., and D.J. Molden (1983). Artificial Groundwater Recharge, San Luis Valley, Colorado. Colorado Water Resources Research Institute, Colorado State University. Completion Report No. 123.

SWAG (Sustainable Water Augmentation Group) (2023). A Brief Water History of the San Luis Valley. https://www.swagwater.com/the-area-brief-water-history-of-the-area/

Swidinsky, A. & El-Kaliouby, H. (2013) Time-lapse transient electromagnetic monitoring of a water infiltration experiment: an application to the Central Avra Valley recharge basin, Tucson, Arizona. *SEG Technical Program Expanded Abstracts 2013: Society of Exploration Geophysicists SEG Technical Program Expanded Abstracts*, 4439–4443.

USGS (2020). USGS_LPC_CO_SanLuisJuanMiguel_2020_D20. U.S. Geological Survey, U.S. Department of the Interior.

Wasiolek, M. (1995). *Subsurface Recharge to the Tesuque Aquifer System from Selected Drainage Basins along the Western Side of the Sangre de Cristo Mountains Near Santa Fe, New Mexico*. Water Resources Investigations Report 94-4072. Denver: US Geological Survey.

Watlet, A., Kaufmann, O., Triantafyllou, A., Poulain, A., Chambers, J. E., Meldrum, P. I., Wilkinson, P. B., Hallet, V., Quinif, Y., Van Ruymbeke, M., and Van Camp, M. (2018). Imaging groundwater infiltration dynamics in the karst vadose zone with long-term ERT monitoring, Hydrol. Earth Syst. Sci., 22, 1563–1592, https://doi.org/10.5194/hess-22-1563-2018.

Woessner, W. W. and E.P. Poeter (2020). Hydrogeologic Properties of Earth Materials and Principles of Groundwater Flow. The Groundwater Project, Guelph, Ontario, Canada.

Worthington, P.F. (1993). The uses and abuses of the Archie equations, 1: The formation factor-porosity relationship. Journal of Applied Geophysics, 30(3), pp. 215-228. https://doi.org/10.1016/0926-9851(93)90028-W.

Xiao, L., G. Fiandaca, P. K. Maurya, A. V. Christiansen, and L. Lévy. (2022). Three-dimensional time-lapse inversion of transient electromagnetic data, with application at an Icelandic geothermal site. Geophysical Journal International, 231, 584–596, doi: 10.1093/gji/ggac206.

Zeigler Geologic Consulting LLC, Mosca-Hooper CD, & Hasbrouck Geophysics (2020). San Luis Valley: Recharge Optimization Project. https://soilcarboncoalition.org/html/slv/rop.html

APPENDIX A – SUPPLEMENTARY DATA

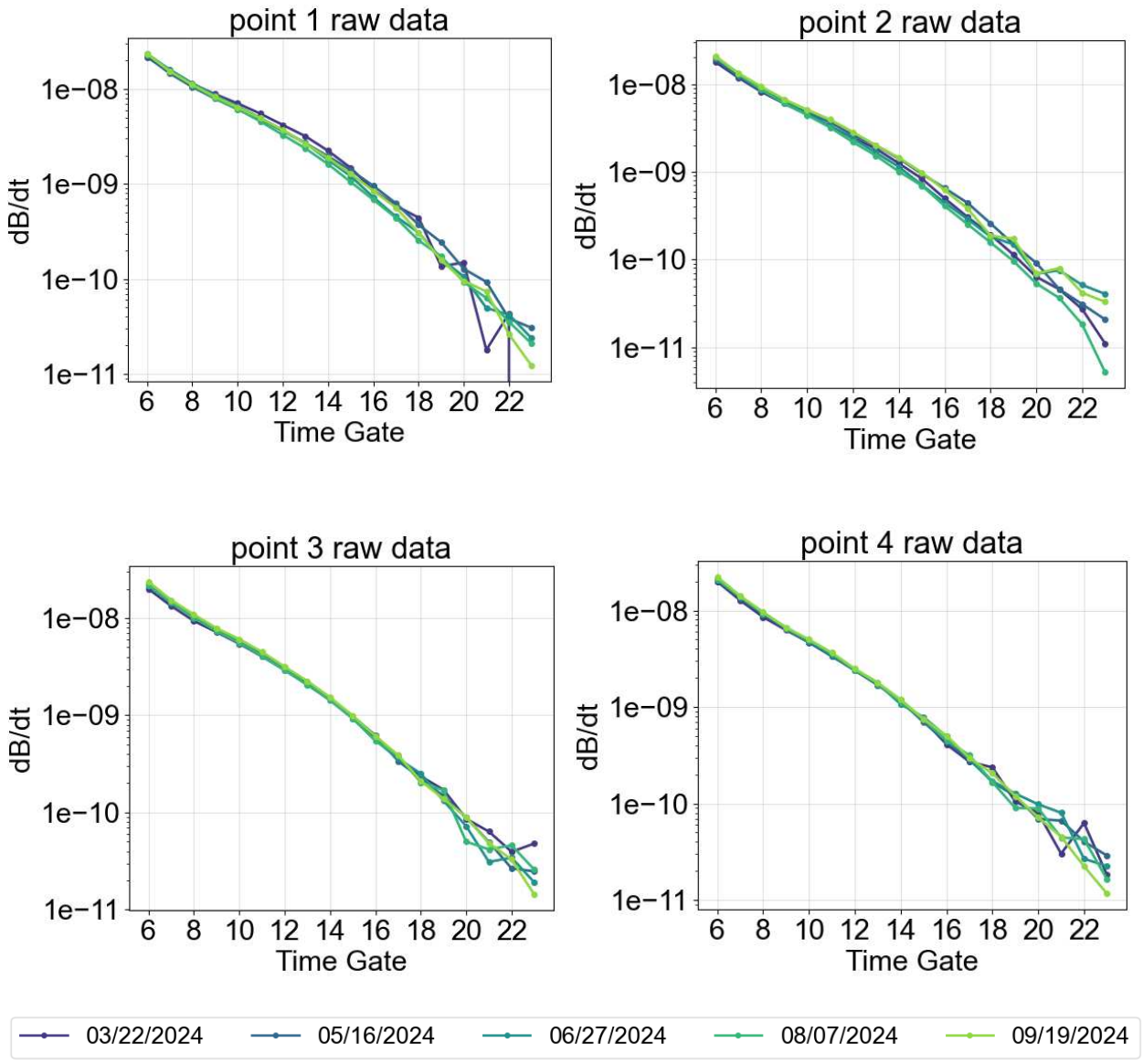

Figure A1: Plots showing raw data from four individual soundings. The locations of the soundings are shown in Figure 11 in the main text. Similarities in raw data across datasets could be indicative of inversion artifacts.

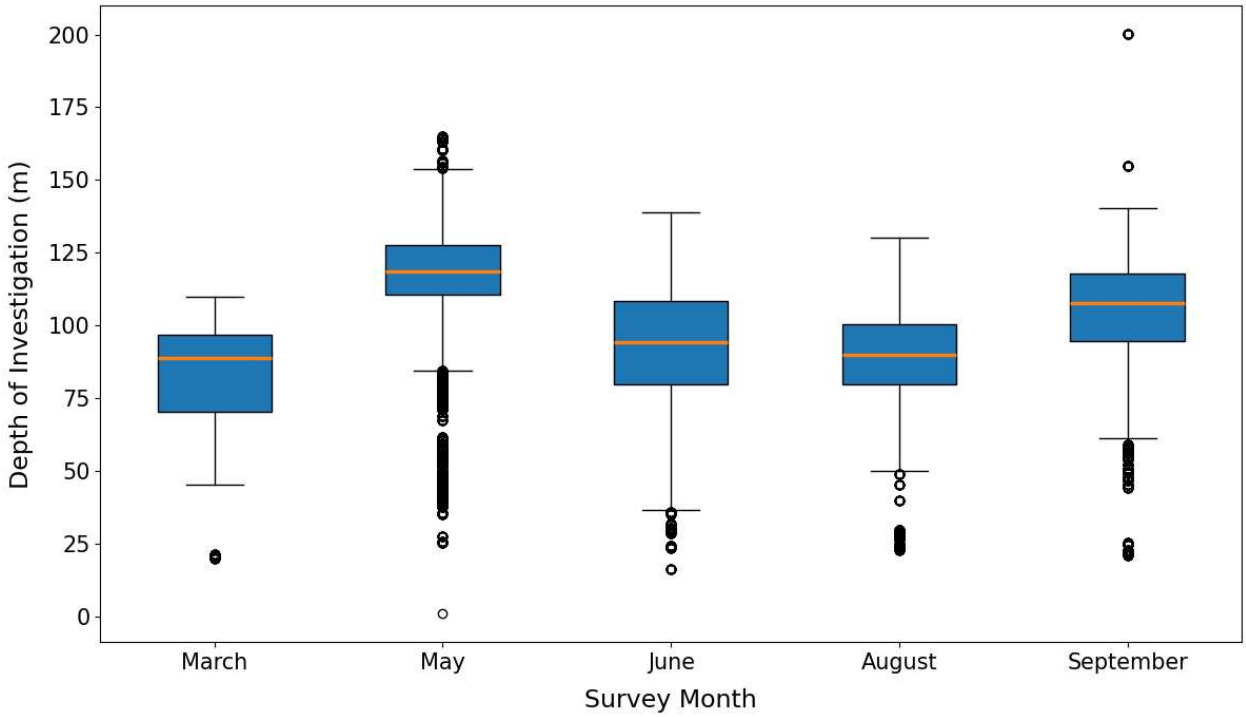

Figure A2: Distribution of depth of investigation (m) of tTEM surveys. Orange lines represent the medians of the distributions.

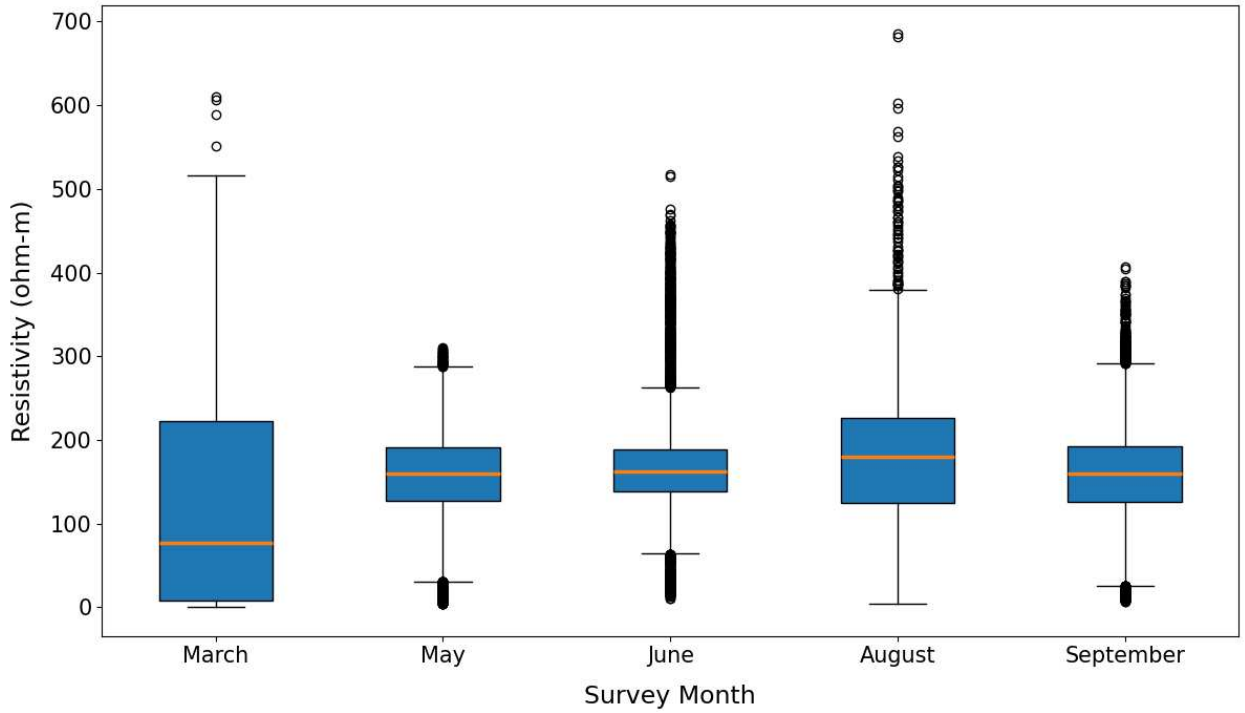

Figure A3: Distribution of resistivity values (ohm-m) from tTEM surveys. Orange lines represent the medians of the distributions. The area values were acquired from is shown below in Figure A4.

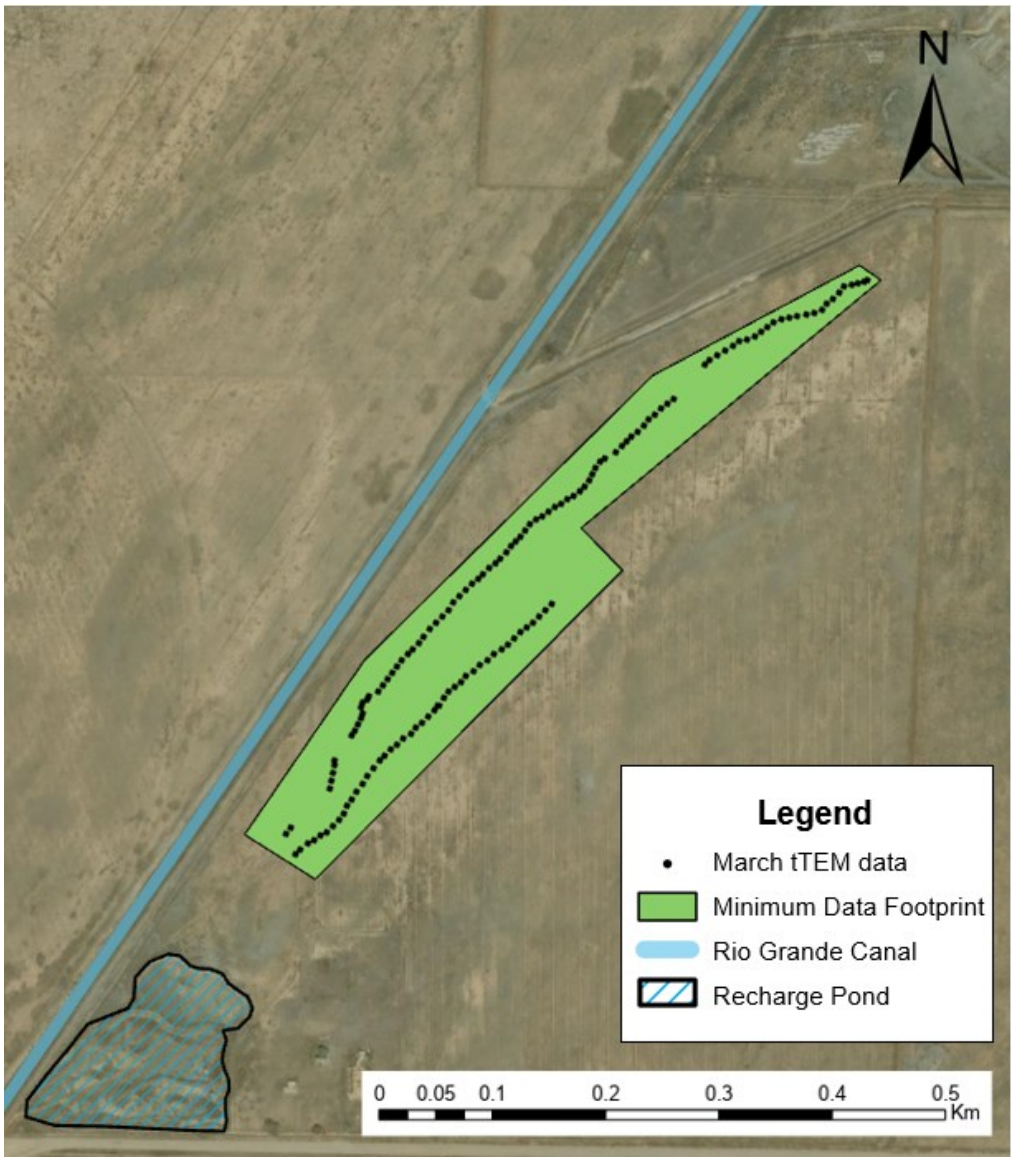

Figure A4: Map showing location of values pulled from each survey for Figure A3. Imagery source: ESRI World Imagery.

Figures A5, A6, and A7 show resistivity with depth for single tTEM soundings selected across datasets ("soundings 2, 3, and 4"). The locations of selected soundings are indicated in yellow in Figure 11 in the main text. Soundings from each dataset were selected as close as possible to one another, with a maximum separation distance of 15 m. The blue dashed line indicates the estimated depth of the water table in March 2024. Depth to the water table fluctuated over the course of the season.

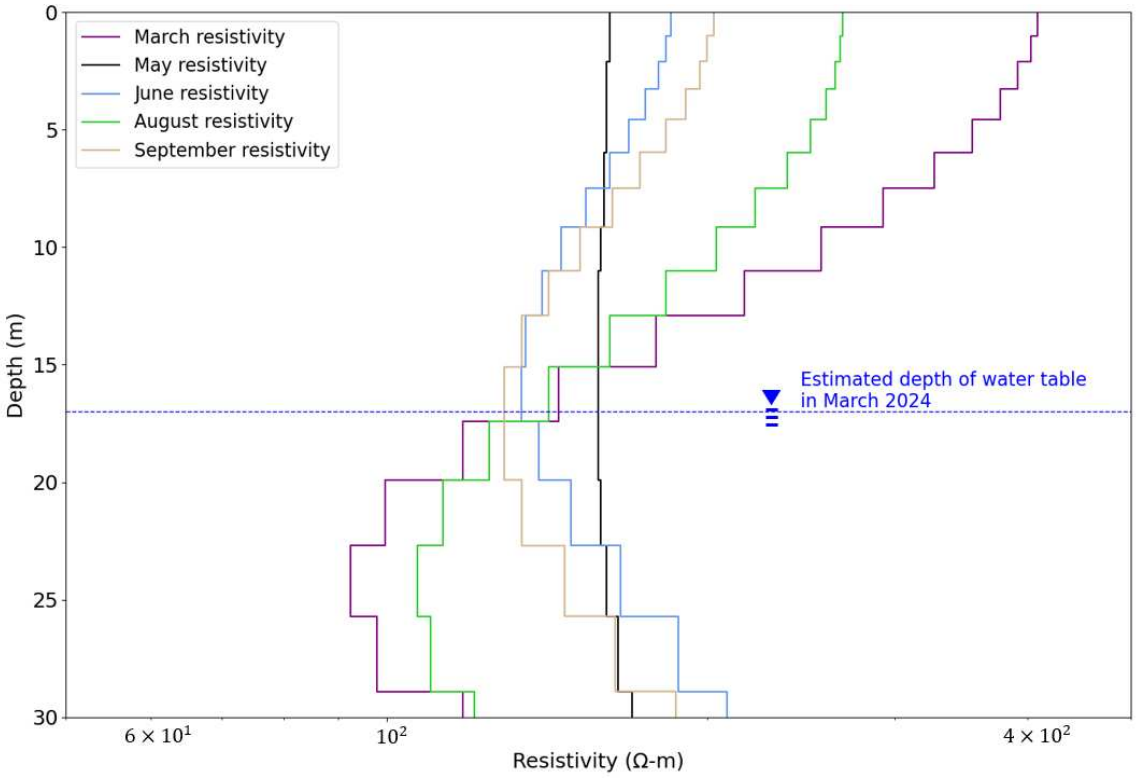

Figure A5: resistivity values from Workbench inversion compared to estimated depth of water table at sounding 2.

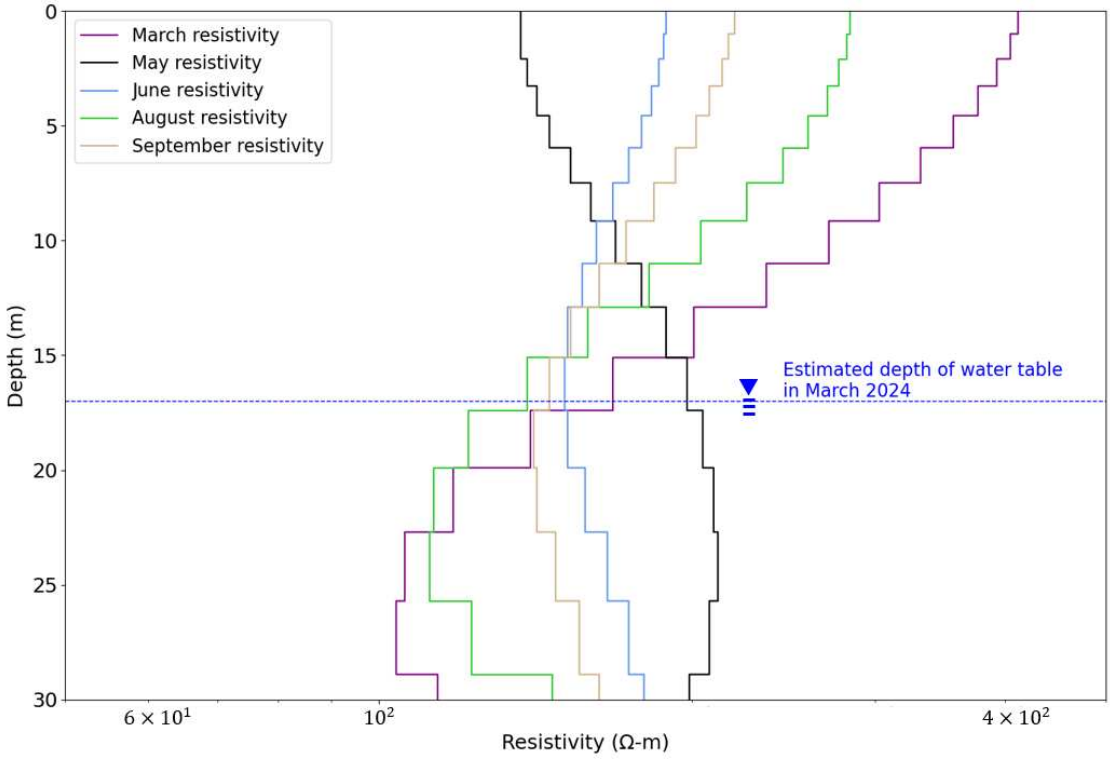

Figure A6: resistivity values from Workbench inversion compared to estimated depth of water table at sounding 3.

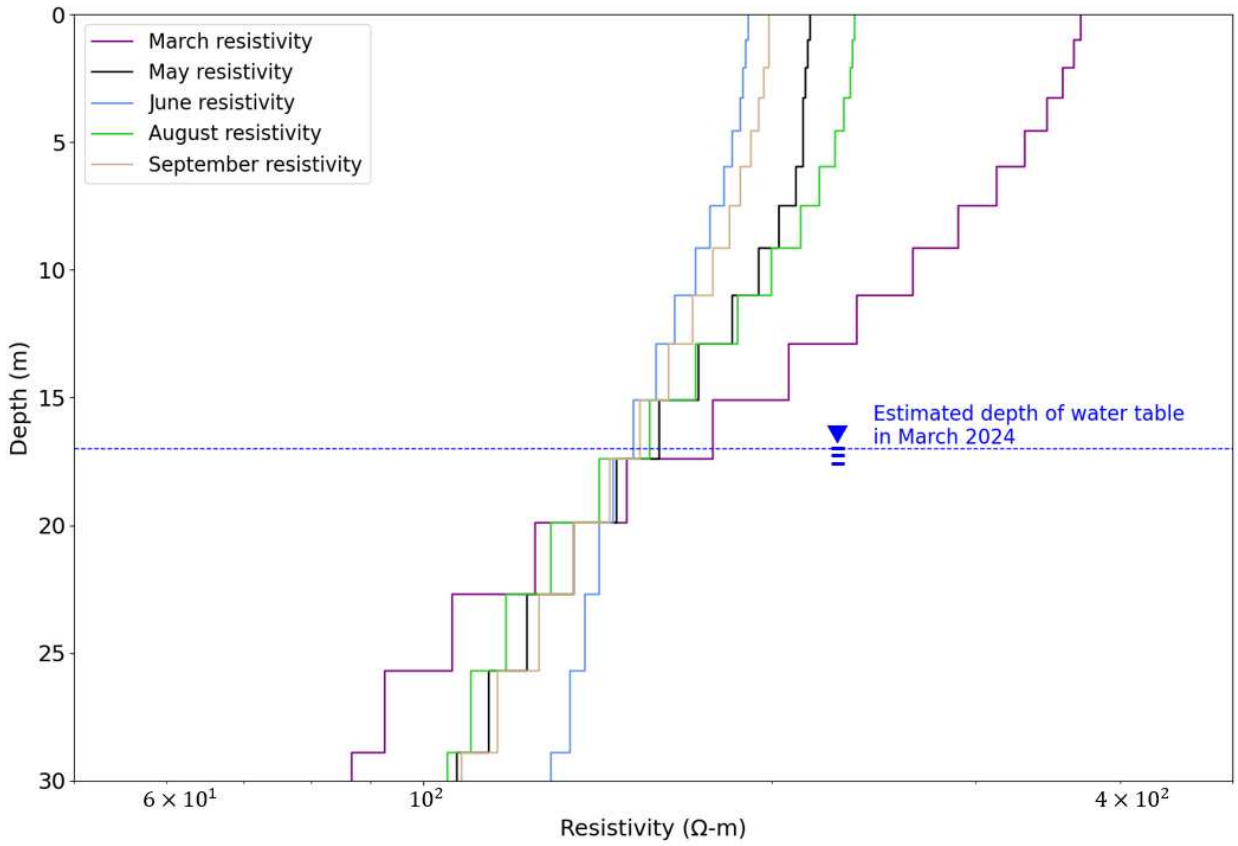

Figure A7: resistivity values from Workbench inversion compared to estimated depth of water table at sounding 4.

Figures A8 and A9 show resistivity values along the transects parallel and perpendicular to the Rio Grande Canal, respectively, at a depth of 5 m.

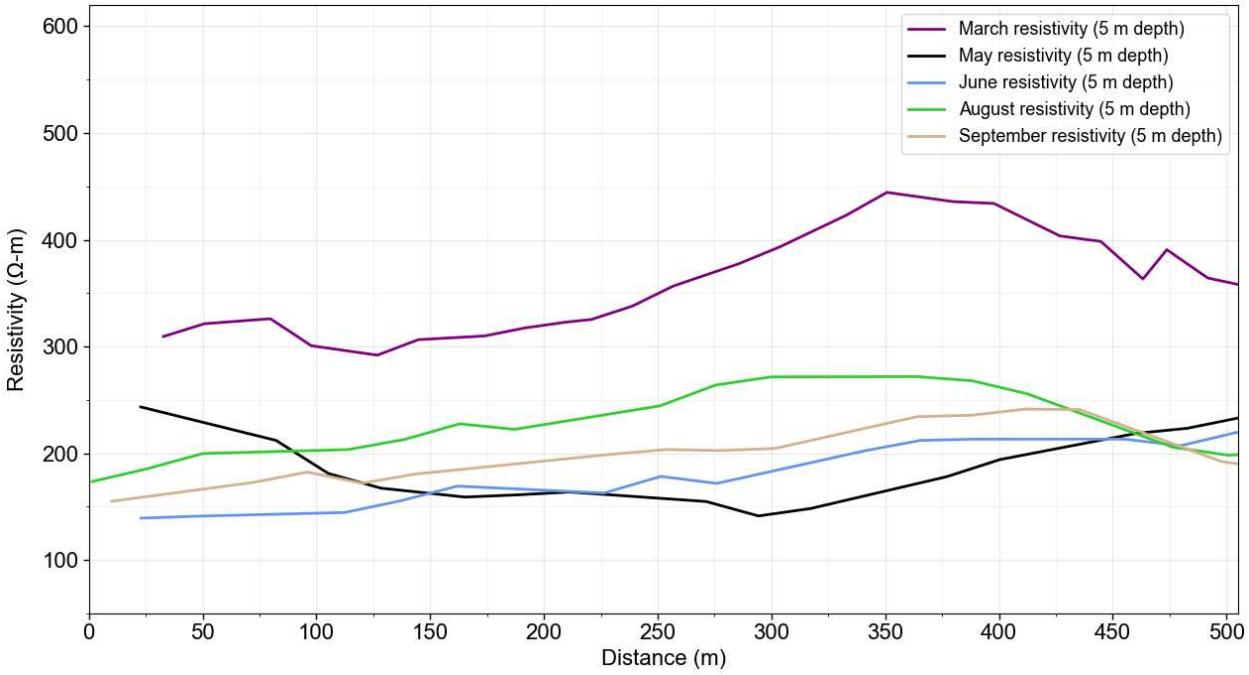

Figure A8: resistivity values from tTEM surveys at 5 m depth, located along parallel transect shown in Figure 11 in the main text.

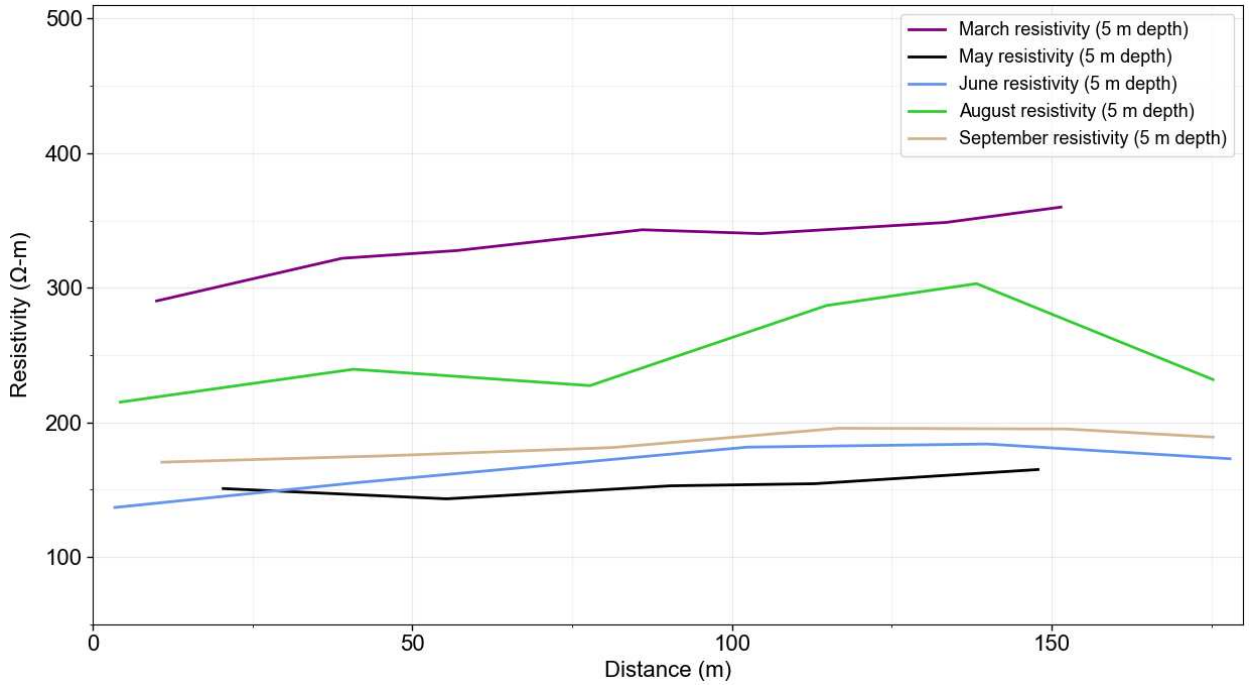

Figure A9: resistivity values from tTEM surveys at 5 m depth, located along perpendicular transect shown in Figure 11 in the main text. Distance on the x-axis goes from northwest to southeast, increasing in distance away from the canal.

APPENDIX B – STATISTICAL ANALYSES

Table 5 shows the model parameters used in semivariograms for kriging. Semivariograms for all datasets used a subset size of 100 and 100 simulations. In this method, the range, nugget, and sill are calculated automatically in ArcGIS Pro.

Table 5: Model parameters used in semivariograms for 3D empirical Bayesian kriging

Dataset	Semivariogram Model Type	Elevation Inflation Factor	Major Semiaxis (search neighborhood)
March 2024	K-Bessel	14.8	104.4
May 2024	K-Bessel	4.89	35.8
June 2024	K-Bessel	3.56	53.6
August 2024	K-Bessel	3.85	56.6
September 2024	K-Bessel	5.74	77.1

Figures B1-B5 below show the empirical distributions of semivariograms for each tTEM dataset. In each plot, the blue lines represent semivariograms, and the blue crosses represent empirical semivariances. The median of the distribution is shown with a solid red line, and the 25th and 75th percentiles are shown with red dashed lines.

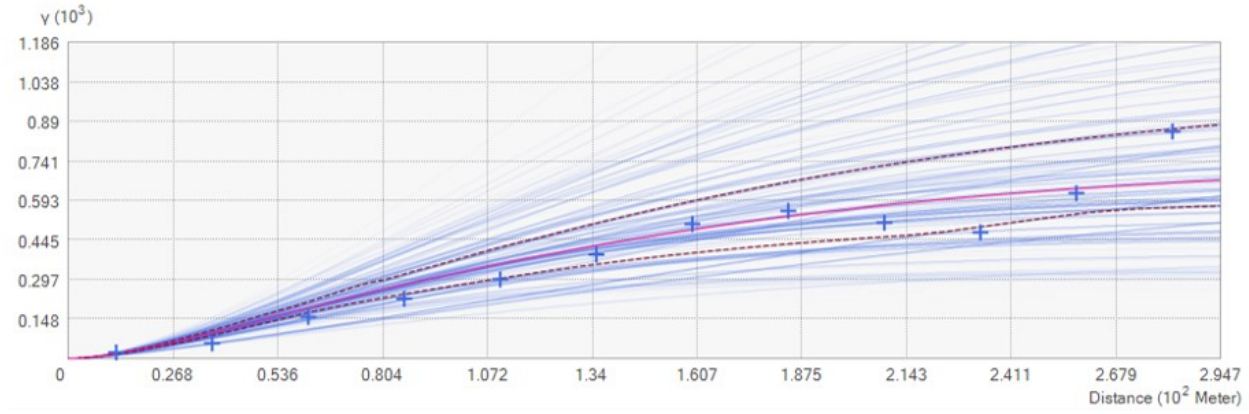

Figure B1: Empirical distribution of semivariograms for kriging of March tTEM data.

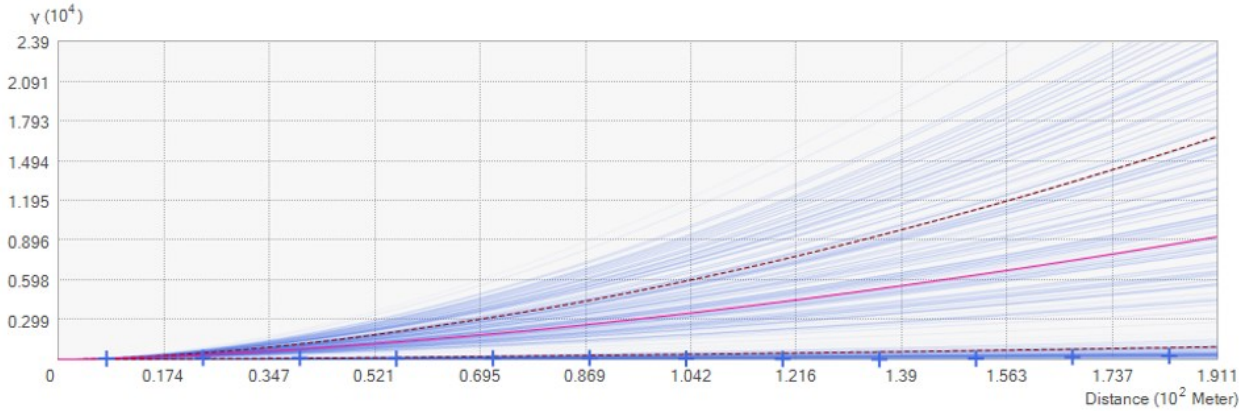

Figure B2: Empirical distribution of semivariograms for kriging of May tTEM data.

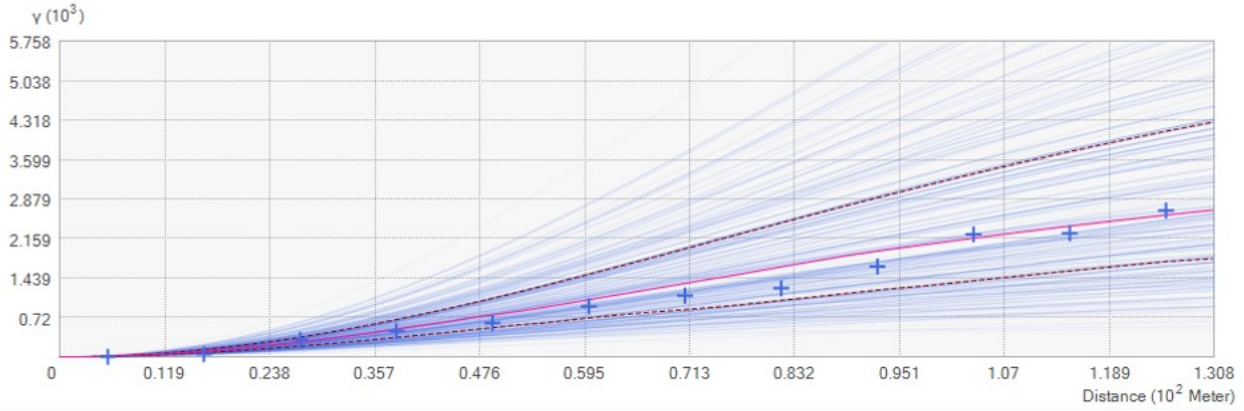

Figure B3: Empirical distribution of semivariograms for kriging of June tTEM data.

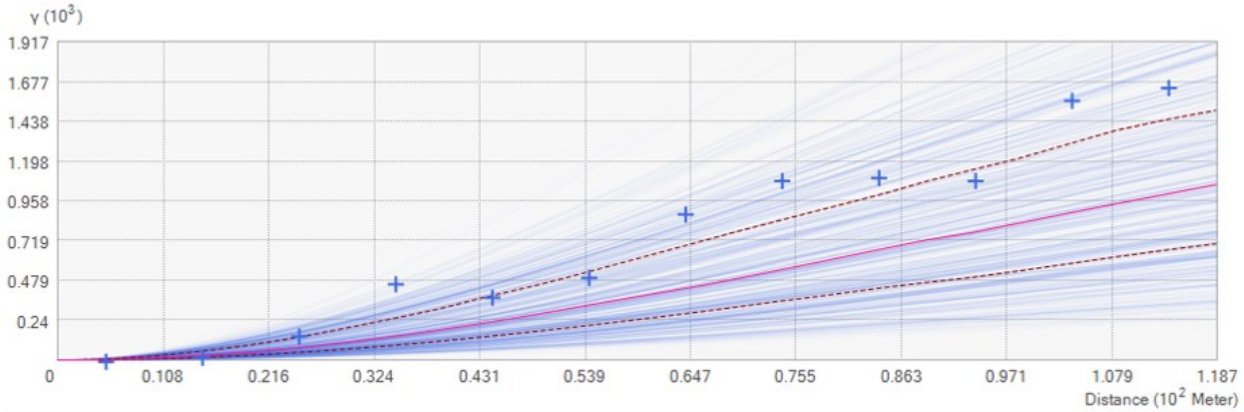

Figure B4: Empirical distribution of semivariograms for kriging of August tTEM data.

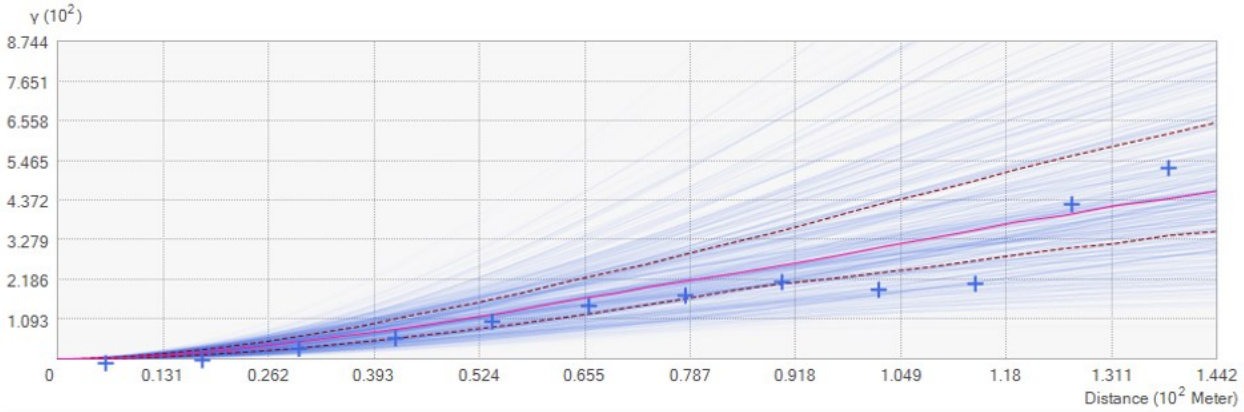

Figure B5: Empirical distribution of semivariograms for kriging of September tTEM data.

Figure B6 shows interpolated groundwater levels based on monitoring well data collected in September 2024. Interpolation was completed using ordinary kriging with a Gaussian variogram model. Results represent an estimate of the regional water table, independent of the effects of managed recharge.

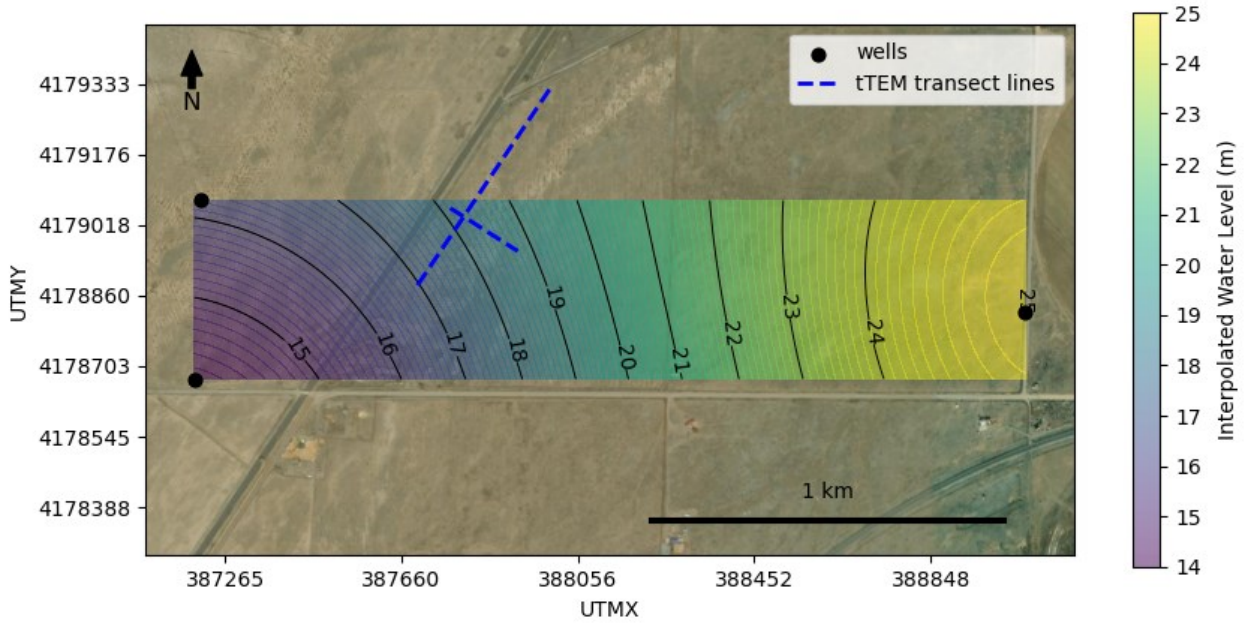

Figure B6. Kriging interpolation of measured well water levels (using water level data from September). Water levels are in units of meters below the ground surface. Imagery sources: ESRI World Imagery.

The semivariogram model parameters used for kriging water level data are shown in Table 6.

Table 6: Model parameters used in semivariograms for 3D empirical Bayesian kriging

Parameter	Value
Sill	50.2 m
Range	2359 m
Nugget	negligible

APPENDIX C – RESISTIVITY CALCULATIONS

Equation (1) shows Archie's law (1942), used to relate the resistivity of a porous rock to its pore water resistivity, porosity, and degree of saturation:

$$\rho_0 = \alpha \rho_f \phi^{-m} S^{-n} \tag{1}$$

In this equation, ρ_0 is the resistivity of a porous rock, ρ_f is the pore water resistivity, ϕ is the porosity, and S is the saturation, or the fraction of the voids filled with water. . The cementation exponent m, reservoir constant α, and saturation exponent n are site-specific material constants. Eq. (1) was applied to characterize the soil type at the study site based on measured resistivity values. Table 7 and Table 8 show ranges of values referenced for pore water resistivity and material constants, respectively. A pore water resistivity of 139 ohm-m was used for ρ_f, and ρ_0 values were determined using resistivity data from the tTEM surveys (shown in Figures 13 and 14 in the main text). An α value of 0.5 and m value of 1.3 were used based on ranges in Garba et al. (2019). An n value of 2 was used based on Archie (1942), and saturation (S) values of 0.1 and 1 were used for the unsaturated and saturated zones, respectively.

Table 7: Measured conductivity of water sampled from various sources of recharge and well. Measurements were made in September 2024.

Source of Sample	Conductivity (mS/cm)	Resistivity (ohm-m)	Temperature (°C)
Rio Grande Canal	0.056	178	14.8
Lateral 1	0.049	201	11.6
Lateral 1e	0.052	190	13.9
Lateral 5	0.054	184	14.8
Lateral 5a	0.053	187	14.8
Well near Lacy Site	0.072	139	13.1

Table 8: Typical ranges of cementation exponent and tortuosity from the literature (Worthington 1993)

Lithology	α	m	References
Sandstone	0.47-1.8	1.64–2.23	Hill and Milburn (1956)
	0.62-1.65	1.3–2.15	Carothers (1968)
	1.0-4.0	0.57–1.85	Porter and Carothers (1970)
	0.48-4.31	1.2–2.21	Timur et al. (1972)
	0.004-17.7	0.02–5.67	Gomez-Rivero (1976)

Table 9 shows calculated ranges of resistivity based on Eq. () and a range of porosity values appropriate for a sandy lithology. Porosity values were based on ranges shown in Table 10. The calculated resistivity values were compared to observed resistivity from tTEM surveys to characterize the soil types for ranges of observed resistivity values.

Table 9: Calculated resistivity values with corresponding porosity and soil types. Average values for porosity and resistivity are show in parentheses.

Soil Type	Porosity Range (%)	Calculated Resistivity (ohm-m) (saturated conditions)	Calculated Resistivity (ohm-m) (unsaturated conditions)
Gravel	25-44 (35)	202-421 (277)	20,200-42,000 (27,700)
Coarse sand	31-46 (39)	191-319 (240)	19,100-32,000 (24,000)
Fine sand	25-53 (39)	159-421 (236)	15,900-42,000 (23,600)

Table 10: Typical ranges of porosity for common earth materials (Woessner and Poeter, 2020)

Total Porosity Range of Some Common Earth Materials (Percent)	
Material	**Range Total Porosity (%)**
Unconsolidated Sediments	
Clay	45-55
Silt	35-50
Fine-sand	26-50
Coarse-sand	30-45
Gravel	25-35
Sand and gravel	20-30
Glacial till	20-30
Consolidated Sediments	
Shale	1-10
Siltstone	20-40
Sandstone	5-30
Limestone and dolomite	1-25
Karstic limestone	5-35

Figure C1 shows ranges of resistivity values for various rock types.

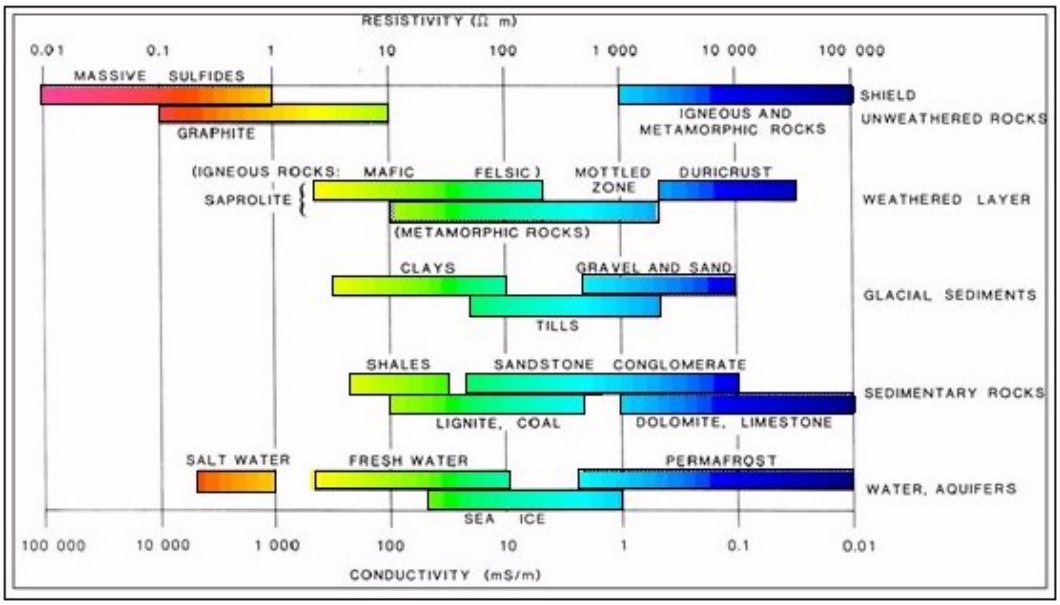

Figure C1: Resistivity ranges of various rock types (Palacky, 1987).

Table 11 shows ranges of resistivity values for common soil types.

Table 11: Resistivity values for common soil types (Anthony 2006; Knight et al., 2018; Li et al., 2024).

Material	Resistivity (ohm-m)
Saturated Clay	1-12
Dry Clay	<25
Saturated Sand and Gravel	>22
Dry Sand	>26
Saturated Sandy Clay/Clayed Sand	12-22
Dry Sandy Clay/Clayed Sand	25-31

Based on the ranges of resistivity values expected for sands and silt materials, resistivity values observed from tTEM data were interpreted as the lithologies shown in Table 12.

Table 12: Observed resistivity from tTEM data with interpreted lithologies.

Soil Type	Observed Resistivity (ohm-m)
Silty sand	100
Clean sand	>200

APPENDIX D – GROUNDWATER AND WELL DATA

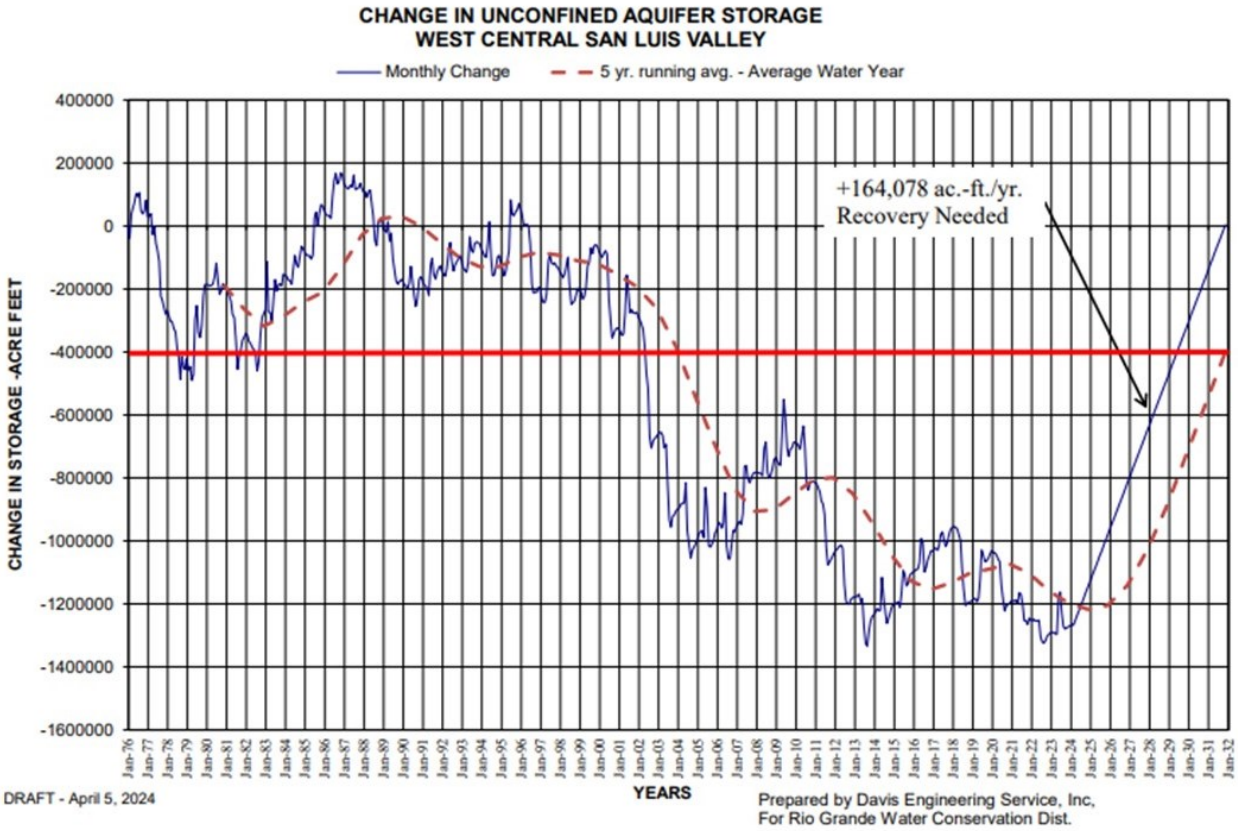

Figure D1: Change in unconfined aquifer storage in the West Central San Luis Valley, 1976-2032 (data extent is through Jan. 2024). From RGWCD (2024).

AUG 24 1961

Form F (Rev.)
7-57/5M

STATE OF COLORADO
DIVISION OF WATER RESOURCES
OFFICE OF THE STATE ENGINEER, GROUND WATER SECTION

MAR 25 1960
GROUND WATER SECT.
COLORADO
STATE ENGINEER

REGISTRATION NO. 10326 (10326) OF WELL

Registrant Jessie L. Bennington Date 3/24/1960

P.O. Address Center, Colo.

WELL DATA

Depth 90 ft. Diameter 20 in.

Casing: 6 ft. Plain; 84 ft. Perfor.

Static Water Level 9 ft. from top

Yield 1500 (gpm)(cfs) from 50 ft.

Used for Irrigation on/at

SE¼ SE¼ Section 35 T41N R66E NM
(legal description of land or site)

Water conveyed by Ground, size 10 in

PUMP DATA

Type Turbine Size 10 in

Driven by Gas Engine at 1400 RPM

Well was first used Aug, 1943
cfs

for Irrigation using 1500 gpm

Well enlarged _____, 19__ to
deepened

_____(gpm)(cfs)(ft)

LOG SHOULD BE GIVEN ON REVERSE SIDE IF AVAILABLE

Not Available

WELL LOCATION

County Saguache 55

SE ¼ SE ¼ Section 35

Twp. 41N, Rge. 6E, NM PM

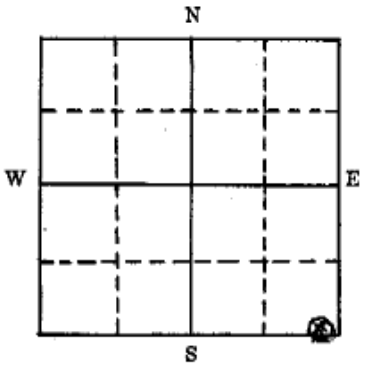

WELL TO BE LOCATED AS ACCURATELY AS POSSIBLE WITHIN A SMALL SQUARE WHICH REPRESENTS 40 ACRES; OR IF IN A TOWN OR SUBDIVISION FILL IN THE FOLLOWING:

_____
Town or Subdivision

_____
Street address or Lot and Block

The above well (has) (has not) been registered in the Office of the State Engineer prior to May 1, 1957. If Registered give Filing No. _____.

If NOT Registered prior to May 1, 1957, a $5.00 filing fee accompanies this form.

The above statements are true and correct to the best of my knowledge and belief.

Subscribed and Sworn before me

this 24th day of March, 1960.

My commission expires Feb. 14-1962

(SEAL) Thelma B. Gardner
Notary Public

Jessie L. Bennington
Registrant

SEE 49798-F

FOR STATE ENGINEER'S USE

Located in 3-20 district, Saguache County for Irrigation

Registration No. 1031 in 3-20, on March 25, 1960

Figure D2: Lacy #3 well permit (driller's log not available).

FORM NO. GWS-31 04/2005

WELL CONSTRUCTION AND TEST REPORT
STATE OF COLORADO, OFFICE OF THE STATE ENGINEER
1313 Sherman St., Room 818, Denver, CO 80203
Phone – Info (303) 866-3587 Main (303) 866-3581
Fax (303) 866-3589 http://www.water.state.co.us

RECEIVED
DEC 26 2006
WATER RESOURCES STATE ENGINEER COLO.

For Office Use Only
RECEIVED
DEC 20 2006
WATER RESOURCES STATE ENGINEER ALAMOSA

1. **WELL PERMIT NUMBER:** OH9798 F

2. **WELL OWNER INFORMATION**
NAME OF WELL OWNER: James & Lynn Lacy
MAILING ADDRESS: HH897 Cr. D
CITY: Center STATE: CO ZIP CODE 81125
TELEPHONE NUMBER: ( )

3. **WELL LOCATION AS DRILLED:** NE 1/4, SE 1/4, Sec. 35, Twp. 41 ☒ N or ☐ S, Range 8 ☒ E or ☐ W
DISTANCES FROM SEC. LINES: 1350 ft. from ☐ N or ☒ S section line and 750 ft. from ☒ E or ☐ W section line.
SUBDIVISION: _____ LOT ____ BLOCK ____ FILING (UNIT) ____
Optional GPS Location: GPS Unit must use the following settings: Format must be **UTM**, Units must be **meters**, Datum must be **NAD83**, Unit must be set to **true N**, ☐ Zone 12 or ☐ Zone 13
Owner's Well Designation: _____
Easting: _____
STREET ADDRESS AT WELL LOCATION:
Northing:

4. GROUND SURFACE ELEVATION 7700 feet
DRILLING METHOD Cable Tool
DATE COMPLETED 10/12/1998 TOTAL DEPTH 150 feet
DEPTH COMPLETED feet 150

5. GEOLOGIC LOG:

Depth	Type	Grain Size	Color	Water Loc.
2	Top Soil			
2'-80'	rock & Sand	3" to ¼"		
80'-100'	Sand			
100'-102	Clay		Brown	
102'-150'	Sand			

6. HOLE DIAM (in.)

	From (ft)	To (ft)
24"	0	150'

7. PLAIN CASING:

OD (in)	Kind	Wall Size (in)	From (ft)	To (ft)
16"	Steel	.217	+1	80'

PERFORATED CASING: Screen Slot Size (in): 100

16"	Steel	.217	80'	150

8. FILTER PACK:
Material rock
Size ¾" - 1"
Interval 0' - 150'

9. PACKER PLACEMENT:
Type _____
Depth _____

10. GROUTING RECORD

Material	Amount	Density	Interval	Placement
Cement	Hyrnds	Neat	8'-20'	Pumped

Remarks: _____

11. DISINFECTION: Type HTH Amt. Used NOE

12. WELL TEST DATA: ☐ Check box if Test Data is submitted on Form Number GWS 39 Supplemental Well Test.
TESTING METHOD Turbine
Static Level 50' ft. Date/Time measured: 10/20/1998 Production Rate 700 gpm.
Pumping Level 100' ft. Date/Time measured _____ Test Length (hrs) 8
Remarks:

13. I have read the statements made herein and know the contents thereof, and they are true to my knowledge. This document is signed and certified in accordance with Rule 17.4 of the Water Well Construction Rules, 2 CCR 402-2. [The filing of a document that contains false statements is a violation of section 37-91-108(1)(e), C.R.S., and is punishable by fines up to $5000 and/or revocation of the contracting license.]

Company Name: Beringer & Sons Irrigation | Phone: (719) 754-3555 | License Number: 7713
Mailing Address: Box 368 Center CO 81125
Signature: _____ | Print Name and Title: Ronald Beringer / Pres | Date: 11/4/98

Figure D3: Lacy #4 well log.

FORM NO. GWS-31 10/94

WELL CONSTRUCTION AND TEST REPORT
STATE OF COLORADO, OFFICE OF THE STATE ENGINEER

For Office Use only RECEIVED
RECEIVED JAN 25 1999
NOV 12 1999
WATER RESOURCES STATE ENGINEER COLO

1. WELL PERMIT NUMBER 213766

2. OWNER NAME(S) RIO GRANDE WATER CONSERVATION DISTRICT
Mailing Address 10900 E Hwy 160
City, St. Zip Alamosa Co. 81101
Phone ( )

3. WELL LOCATION AS DRILLED: SE 1/4 SE 1/4, Sec. 28 Twp. 41 N, Range 6 E
DISTANCES FROM SEC. LINES:
600 ft. from South (north or south) Sec. line and 10 ft. from East (east or west) Sec. line. OR NM P.M.
SUBDIVISION: LOT BLOCK FILING(UNIT)
STREET ADDRESS AT WELL LOCATION:

4. GROUND SURFACE ELEVATION ft. DRILLING METHOD AIR ROTARY
DATE COMPLETED 12-15-98 TOTAL DEPTH 130 ft. DEPTH COMPLETED 130 ft.

5. GEOLOGIC LOG:

Depth	Description of Material (Type, Size, Color, Water Location)
0-2	topsoil
2-60	large gravel
60-67	Brown clay
67-82	sand
82-120	medium gravel
120-125	Hard packed gravel
125-133	gravel

6. HOLE DIAM.

(in.)	From (ft)	To (ft)
10	0	12
7	12	130

7. PLAIN CASING

OD (in)	Kind	Wall Size	From(ft)	To(ft)
6 5/8	steel	.188	+2	76
4	PVC	sch 40	+2	89.5

PERF. CASING: Screen Slot Size: .020

4"	PVC	sch 40	89.5	130

8. FILTER PACK:
Material silica sand
Size 8-12
Interval 86-130

9. PACKER PLACEMENT:
Type
Depth

10. GROUTING RECORD:

Material	Amount	Density	Interval	Placement
Cement	2.5sks			
		15gal.	0-12	conductor pipe poured

REMARKS:

11. DISINFECTION: Type hth Amt. Used 5 Ozs.

12. WELL TEST DATA: ☐ Check box if Test Data is submitted on Form No. GWS 39 Supplemental Well Test.
TESTING METHOD Air Lift
Static Level 38.9" ft. Date/Time measured 12-15-98 3:pm, Production Rate 50 gpm.
Pumping level n/a ft. Date/Time measured , Test length (hrs.) 2 hrs.
Remarks Monitoring well

13. I have read the statements made herein and know the contents thereof, and that they are true to my knowledge. [Pursuant to Section 24-4-104 (13)(a) C.R.S., the making of false statements herein constitutes perjury in the second degree and is punishable as a class 1 misdemeanor.]

CONTRACTOR Ken C. Burk of Burk Drilling Inc. Phone (719)852-4845 Lic. No.1137
Mailing Address 1499 N. HWY 285 Monte Vista CO. 81144

Name/Title (Please type or print)	Signature	Date
Ken C. Burk President	Ken C. Burk	12-15-98

Figure D4: RG33B well log.